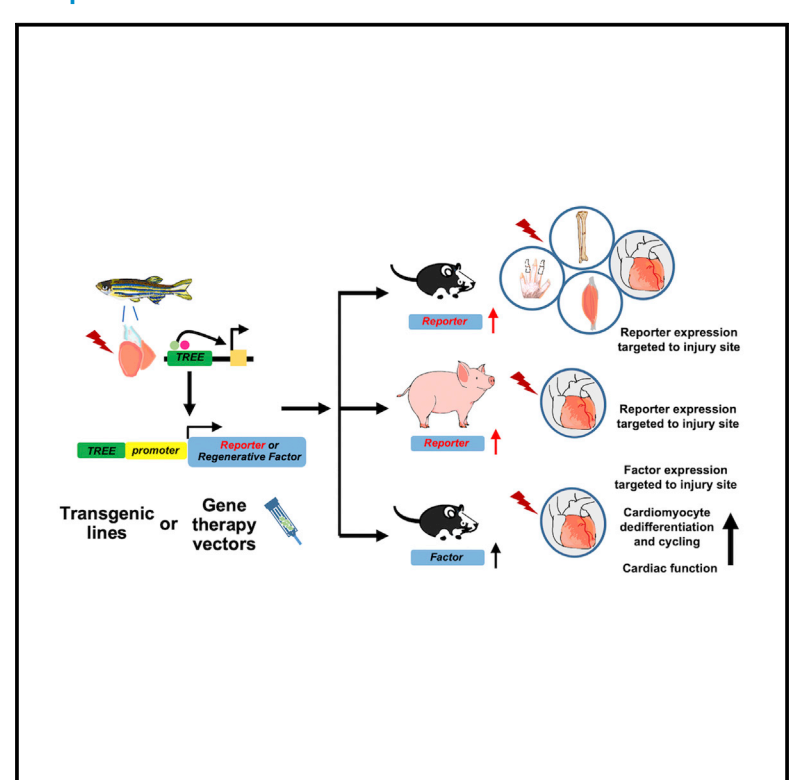
An enhancer-based gene-therapy strategy for spatiotemporal control of cargoes during tissue repair

Graphical abstract



Authors

Ruorong Yan, Valentina Cigliola, Kelsey A. Oonk, ..., Nenad Bursac, Brian L. Black, Kenneth D. Poss

Correspondence

ken.poss@duke.edu

In brief

Yan and Cigliola et al. engineer zebrafish enhancer elements into AAV vectors, illustrating that these constructs can spatiotemporally target gene expression to injury sites of small and large mammals and improve regenerative responses to heart damage. Enhancer-based gene control has the potential to add efficacy and precision to gene therapies for regenerative medicine.

Highlights

- TREEs of zebrafish origin target gene expression to adult mammalian injury sites
- TREEs endow spatiotemporal control of cargoes from systemically delivered AAV vectors
- Control of endogenous genes at injury sites by TREEregulated epigenome editing
- TREE-based YAP delivery boosts cardiac regeneration and function in injured mice







Resource

An enhancer-based gene-therapy strategy for spatiotemporal control of cargoes during tissue repair

Ruorong Yan, 1,2,15 Valentina Cigliola, 1,2,15 Kelsey A. Oonk, 1,2 Zachary Petrover, 8 Sophia DeLuca, 2,4 David W. Wolfson, 1,2,5,6 Andrew Vekstein, 5 Michelle A. Mendiola, 5 Garth Devlin, 5 Muath Bishawi, 4,5 Matthew P. Gemberling, 4,6 Tanvi Sinha,3 Michelle A. Sargent,7 Allen J. York,7 Avraham Shakked,8 Paige DeBenedittis,9

David C. Wendell, ¹⁰ Jianhong Ou, ¹ Junsu Kang, ¹¹ Joseph A. Goldman, ¹² Gurpreet S. Baht, ^{13,14} Ravi Karra, ⁹ Adam R. Williams,⁵ Dawn E. Bowles,⁵ Aravind Asokan,^{1,4,5,6} Eldad Tzahor,⁸ Charles A. Gersbach,^{1,2,4,5,6,14}

Jeffery D. Molkentin,⁷ Nenad Bursac,⁴ Brian L. Black,³ and Kenneth D. Poss^{1,2,6,16,*}

SUMMARY

The efficacy and safety of gene-therapy strategies for indications like tissue damage hinge on precision; yet, current methods afford little spatial or temporal control of payload delivery. Here, we find that tissue-regeneration enhancer elements (TREEs) isolated from zebrafish can direct targeted, injury-associated gene expression from viral DNA vectors delivered systemically in small and large adult mammalian species. When employed in combination with CRISPR-based epigenome editing tools in mice, zebrafish TREEs stimulated or repressed the expression of endogenous genes after ischemic myocardial infarction. Intravenously delivered recombinant AAV vectors designed with a TREE to direct a constitutively active YAP factor boosted indicators of cardiac regeneration in mice and improved the function of the injured heart. Our findings establish the application of contextual enhancer elements as a potential therapeutic platform for spatiotemporally controlled tissue regeneration in mammals.

INTRODUCTION

Gene therapy with recombinant adeno-associated viruses (AAVs) has improved rapidly over recent years and offers persistent, long-term gene expression that has certain advantages over RNA- or protein-based therapies. Methods for preventing or treating the effects of single-gene disorders are clinically approved, and the promise of broader applications appears on the horizon. Current gene therapy is largely focused on gene replacement to address genetically inherited defects that do not typically require precisely regulated expression of therapeutic factors/proteins. For instance, vector dose and route of administration are primary variables taken into consideration in replacement of a secreted enzyme in treating blood-coagulation disorders or certain glycogen-storage disorders.^{2,3} In contrast, many diseases may require regulation of therapeutic gene product, which can be deleterious if expressed continuously in the wrong place at the wrong time. 4,5 While AAV capsid choice can lend moderate tissue specificity to transduced tissues, 6 and promoter fragments direct expression in specific cell types, 7,8 precise spatiotemporal control remains a significant challenge. There is a major unmet need in the field for innovative approaches that



¹Duke Regeneration Center, Duke University, Durham, NC, USA

²Department of Cell Biology, Duke University Medical School, Durham, NC, USA

³Cardiovascular Research Institute, University of California, San Francisco, San Francisco, CA, USA

⁴Department of Biomedical Engineering, Duke University, Durham, NC, USA

⁵Department of Surgery, Duke University School of Medicine, Durham, NC, USA

⁶Center for Advanced Genomic Technologies, Duke University, Durham, NC, USA

Department of Pediatrics, Cincinnati Children's Hospital Medical Center, University of Cincinnati, Cincinnati, OH, USA

Boundary Specifical Properties & Parameter & Parame

⁹Department of Medicine, Duke University Medical Center, Durham, NC, USA

¹⁰Duke Cardiovascular Magnetic Resonance Center, Duke University Medical Center, Durham, NC, USA

¹¹Department of Cell and Regenerative Biology, School of Medicine and Public Health, University of Wisconsin-Madison, Madison, WI, USA

¹²Department of Biological Chemistry and Pharmacology, Ohio State University, Columbus, OH, USA

¹³Duke Molecular Physiology Institute, Duke University School of Medicine, Durham, NC, USA

¹⁴Department of Orthopaedic Surgery, Duke University School of Medicine, Durham, NC, USA

¹⁵These authors contributed equally

¹⁶Lead contact

^{*}Correspondence: ken.poss@duke.edu https://doi.org/10.1016/j.stem.2022.11.012



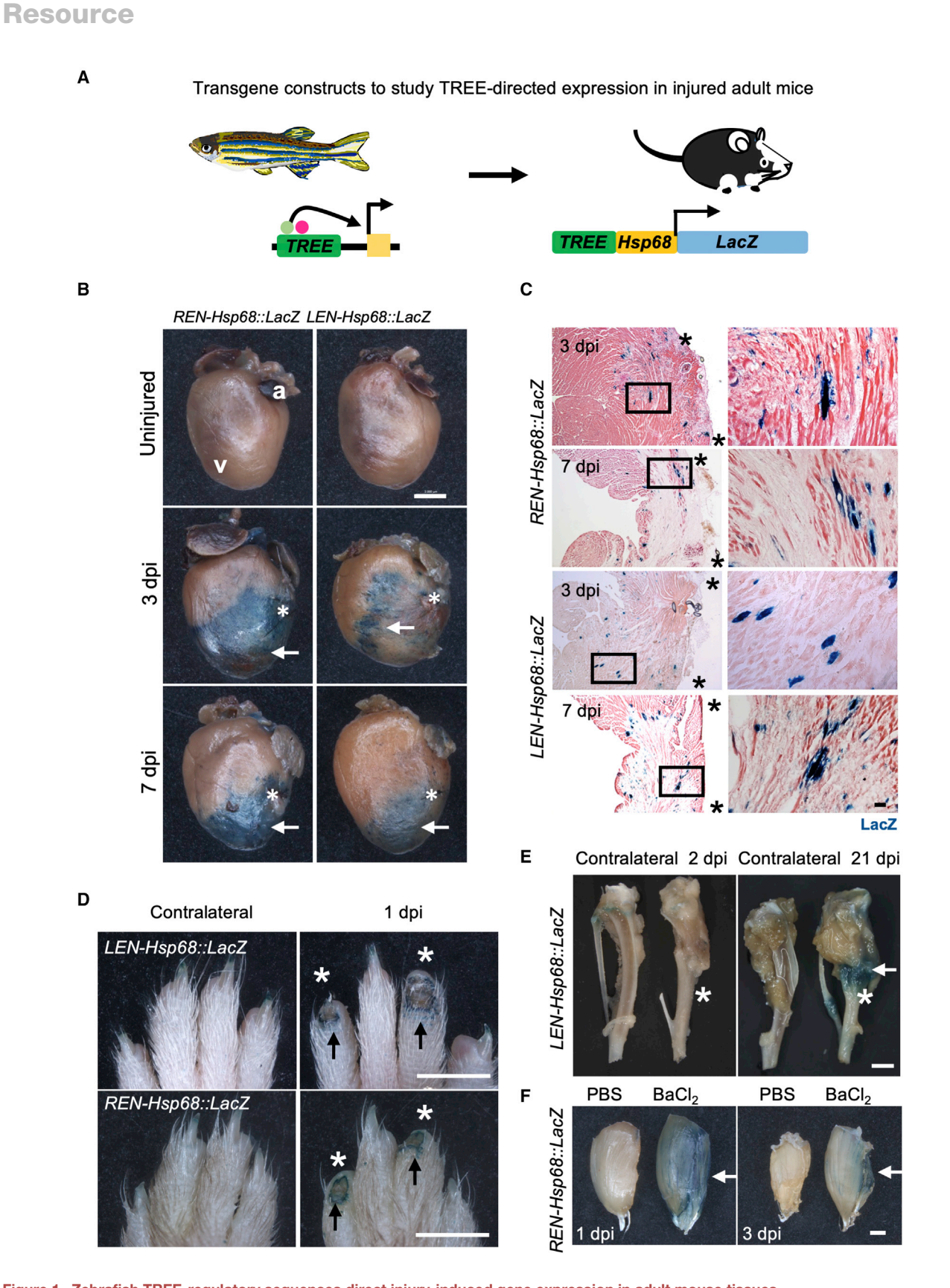


Figure 1. Zebrafish TREE-regulatory sequences direct injury-induced gene expression in adult mouse tissues

(A) Transgene constructs to evaluate the ability of individual zebrafish TREEs to direct expression of a permissive promoter (*Hsp68*) in adult mouse tissues upon injury.



enable the specific targeting of genes to affected subregions of tissue or subpopulations of cells and for reliable and robust methods for control of gene expression within tight time windows.

Regenerative biology may offer an elegant solution to the problem of regulating gene expression. Regeneration involves the rewiring of the expression of hundreds to thousands of genes, shifting programmatic focus of an organ or appendage from pure function to cell proliferation and morphogenesis. 9 Understanding how these changes in gene expression are orchestrated and interpreted is one of the great challenges in the field of regenerative biology. Distally acting regulatory sequences, or enhancers, can direct expression of their target genes and have been predominantly studied as a means for stage- and tissue-specific regulation during embryonic development. Studies in zebrafish have identified tissue regeneration enhancer elements, or TREEs, that can activate expression of their target genes at an injury site, maintain expression during regeneration, and diminish expression as regeneration concludes.¹⁰ TREEs are identifiable by chromatin profiling, which has revealed or suggested similar classes of requlatory elements in Drosophila imaginal wing discs, 11-13 acoel worms, 14 mouse bone, 15 zebrafish and killifish fins, 16-18 and zebrafish hearts 19,20 among other species and tissues. Whereas some enhancers appear to respond to stress or trauma itself, other elements track regeneration weeks after the initial event or can direct gene expression in response to mitogenic stimuli in the absence of tissue damage. 10,19

Context-dependent regulatory sequences represent potential control modules for manipulating expression of pro-regenerative factors in injury sites. Importantly, pro-regenerative factors are expected to be developmentally potent, or even tumorigenic, and would ideally be delivered in a spatially targeted fashion that is initiated by injury and ceases after the resolution of damage. Recent studies have found that TREEs can be engineered to control specific gene cassettes in transgenic animals in a manner that restricts expression throughout life unless a major injury occurs. 10,21 Whereas this type of transgenic rescue was capable of improving regenerative responses in zebrafish, the cross-species recognition of TREEs has only been superficially explored, and it is unknown whether they can be employed to address barriers in mammalian regeneration.

The heart is one of several tissues that are poorly regenerative in adult mammals, and it is a central target of regenerative medicine efforts due to the prevalence and impact of acute myocardial infarction (MI) and heart failure. The principal mechanism for heart regeneration is the proliferation of cardiac muscle cells, which is stimulated after injury in zebrafish and neonatal mice but is negligible in adult mammals. 22,23 Substantial genetic roadblocks to division of adult mammalian cardiomyocytes (CMs)

exist at levels of metabolism, cell-cycle regulation, and chromatin structure.²⁴⁻²⁸ Yet, a number of studies have reported manipulations in transgenic or mutant animals that can increase the regenerative responses of adult murine CMs, including manipulations of cell-cycle factors, mutated oncogenes, and reprogramming factors.^{29–34} Because of the nature of the genes that are manipulated, methods that limit their effects to when and where they are needed—that is, transient expression in the injury border zone-are of great value if relevant targets are to be considered in therapeutic settings.

Here, we tested the ability of zebrafish TREEs to direct the expression of genes to injured tissue in adult mammals. We find a high degree of recognition by murine and porcine tissue. Importantly, TREEs displayed specificity and efficacy when used as gene-therapy modules in systemically delivered recombinant AAV vectors in mice, including the capacity to localize cardiogenic events and improve cardiac function. Our study provides a foundation for new gene-therapy approaches to improve tissue repair in disease settings.

RESULTS

Zebrafish TREEs are injury responsive in adult mouse tissues

To determine if zebrafish TREEs direct gene expression to cardiac injuries in adult mice, we assessed previously described and new transgenic reporter mouse lines generated with constructs containing one of three zebrafish TREEs, a permissive Hsp68 promoter, and a LacZ gene cassette (Figure 1A). The zebrafish TREEs lepb-linked enhancer (LEN), runx1-linked enhancer (103runx1EN or REN), and il11a-linked enhancer (il11aEN)^{10,19} each directed LacZ reporter-gene expression to border-zone tissue following ligation of the left coronary artery (LCA) to generate an MI injury, whereas little or no expression was detectable in uninjured animals (Figures 1B and S1A). Histology indicated increased reporter-gene expression selectively at injury sites at 3 and 7 days post injury (dpi) (Figure 1C). These findings indicate that zebrafish enhancers can target gene expression to injury sites in the adult mammalian heart.

To assess whether zebrafish enhancers direct injury-induced gene expression in other adult tissues, we imparted tibial bone fractures, amputated digits, or injected BaCl2 into skeletal muscle in these transgenic reporter mice. We observed injury-restricted β-galactosidase signals in tibial fracture sites at 21 dpi and at the amputation planes of digits at 1 dpi in LEN-Hsp68::LacZ transgenic animals (Figures 1D and 1E). REN directed LacZ expression at digit amputation planes and injured skeletal muscle (Figures 1D and 1F), whereas no LacZ expression was detectable at digit amputation planes in

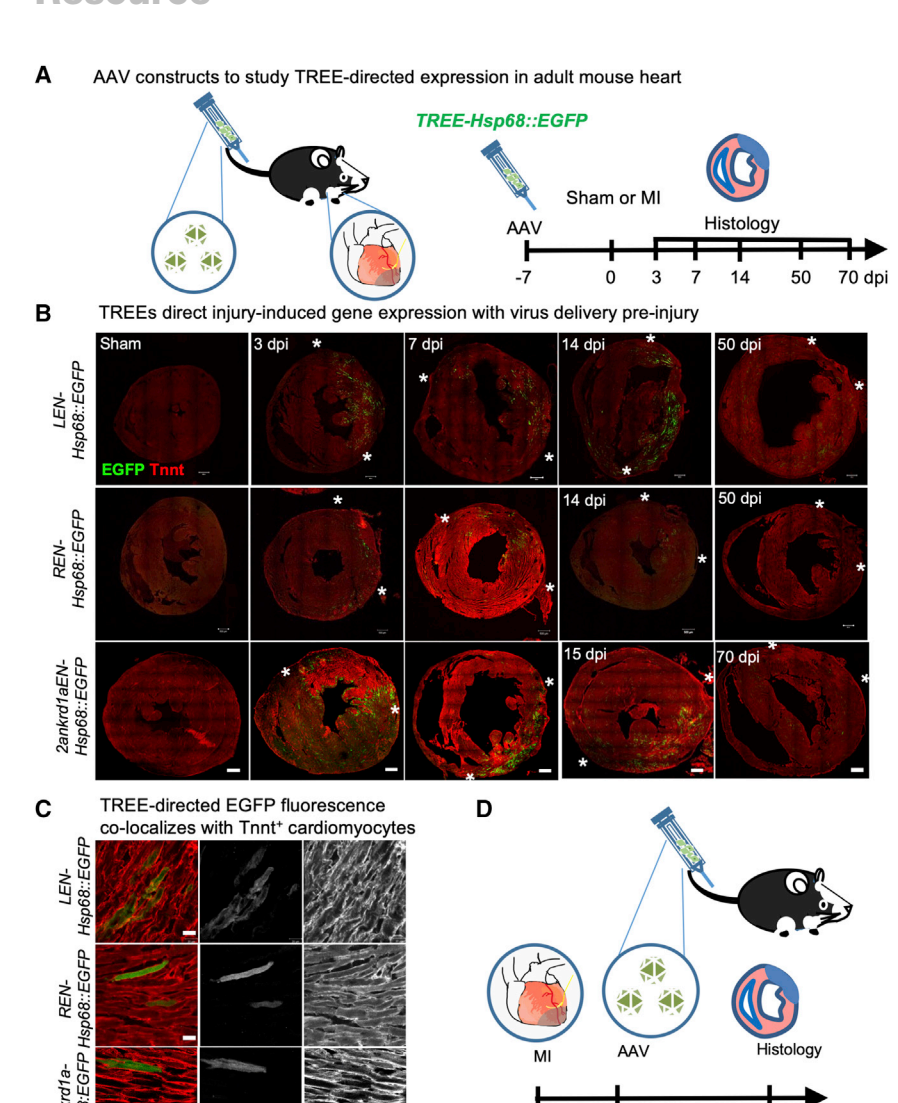
⁽B) Whole-mount images of X-gal-stained adult mouse hearts, with staining (arrowheads) appearing in the area of LCA ligation (asterisks) but not in uninjured hearts. a, atrium; v, ventricle. LEN-Hsp68::LacZ: n = 9, 11, and 6, REN-Hsp68::LacZ: n = 7, 6, and 5 for uninjured, 3 and 7 dpi, respectively. Scale bars, 2 mm. (C) Section images of X-gal-stained adult mouse hearts, with staining appearing in the infarcted area and restricted to the injured site (asterisks). High-magnification view (right) of box in left. Scale bars, 200 µm.

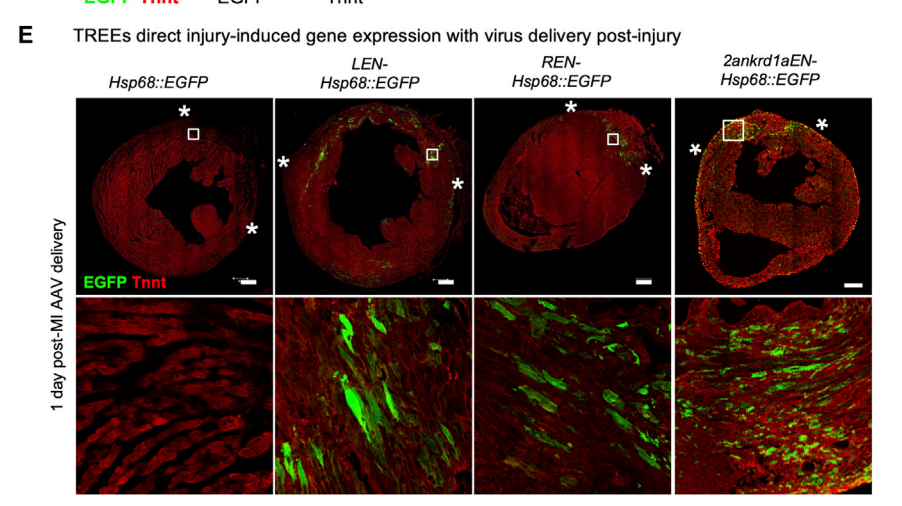
⁽D) Whole-mount images of X-gal-stained digits of adult LEN-Hsp68::LacZ or REN-Hsp68::LacZ mice. Staining (arrows) is evident in amputated digit tips only (asterisks). n = 6 (3) and 8 (4) for LEN-Hsp68::LacZ and REN-Hsp68::LacZ digits (animals), respectively. Scale bars, 2 mm.

⁽E) Whole-mount images of X-gal-stained tibia of adult LEN-Hsp68::LacZ mice 2 and 21 days after tibia fracture. Staining (arrowhead) is evident in fractured site (asterisks) at 21 dpi. n = 5 and 7 for 2 and 21 dpi, respectively. Scale bars, 2 mm.

⁽F) Whole-mount images of X-gal-stained tibialis anterior (TA) muscles of adult REN-Hsp68::LacZ mice 1 and 3 days after BaCl2-induced injury. Staining (arrowheads) is evident in injured TA muscles. n = 5 and 3 for 1 and 3 dpi, respectively. Scale bars, 2 mm.







il11EN-Hsp68::LacZ animals (Figure S1B). Thus, zebrafish enhancers can direct injury-induced expression in a variety of adult mouse tissues.

Figure 2. Zebrafish TREE constructs direct gene expression in injured murine cardiac tissue when delivered by AAV pre- or post-MI

(A) (Left) Schematic for virus delivery and ligation of LCA. (Right) Experimental design in (B) and (C). (B) Section images of hearts after sham or MI injury, from adult mice transduced pre-injury with AAV9 harboring a zebrafish TREE, an Hsp68 minimal promoter, and an EGFP cassette. Fluorescence is induced by injury and restricted to CMs near the MI (asterisks). Tnnt antibody shows nonspecific background at the injury site when stained with fixed heart samples, which is not observed in unfixed heart samples (see Figure 5B). LEN-Hsp68::EGFP: n = 6, 4, 5, 5, and 3, REN-Hsp68::EGFP: n = 6, 4, 4, 3, and 3 for sham, 3, 7, 14, and 50 dpi, respectively. 2ankrd1aEN-Hsp68::EGFP: n = 4, 3, 5, 3, and 3 for sham, 3, 7, 15, and 70 dpi, respectively. LEN-Hsp68:: EGFP, REN-Hsp68::EGFP, and 2ankrd1aEN-Hs p68::EGFP are detectable in MI injury. Scale bars,

(C) TREE-driven EGFP fluorescence co-localizes with Tnnt⁺ cardiomyocytes. Scale bars, 50 μm. (D) Experimental design in (E).

(E) Section images of hearts after MI, from adult mice transduced 1 day post-MI with AAV9 harboring TREE-Hsp68::EGFP or control Hsp68::EGFP. EGFP fluorescence is detectable at the injury sites (asterisks) in each TREE-Hsp68::EGFP group. n = 5, 3, 3, and 4 for LEN-Hsp68::EGFP, REN-Hsp68::EGFP, 2ankrd1aEN-Hsp68::EGFP, and Hsp68::EGFP, respectively. Box from top image is magnified in bottom. Scale bars, 500 μm .

Zebrafish TREEs target transient gene expression to injured mvocardial tissue when delivered by AAV vectors

To explore the activity of zebrafish enhancers in a gene-therapy strategy, we employed AAVs to deliver TREE-based expression modules. We generated AAV serotype 9 (AAV9) vectors with the 3 zebrafish TREEs described above and 3 others (2andkrd1aEN, 22sema3aaEN, and IN13zgc:136858)10,19 (Figures S1C-S1E), fused to a murine Hsp68 promoter and an enhanced green fluorescent protein (EGFP) reporter cassette. We administered each TREE vector systemically to mice by tail vein injection 1 week before MI (Figure 2A). At different time points after MI, hearts were assessed for EGFP expression by immunofluorescence. We estimated the efficiency of transduction at 45%-65% of CMs throughout the border zone and distal areas, based on

quantification of EGFP fluorescence directed by a hybrid form of the chicken β-actin promoter (CBh) delivered on an AAV vector (Figure S2A). Three of the six zebrafish TREEs we tested



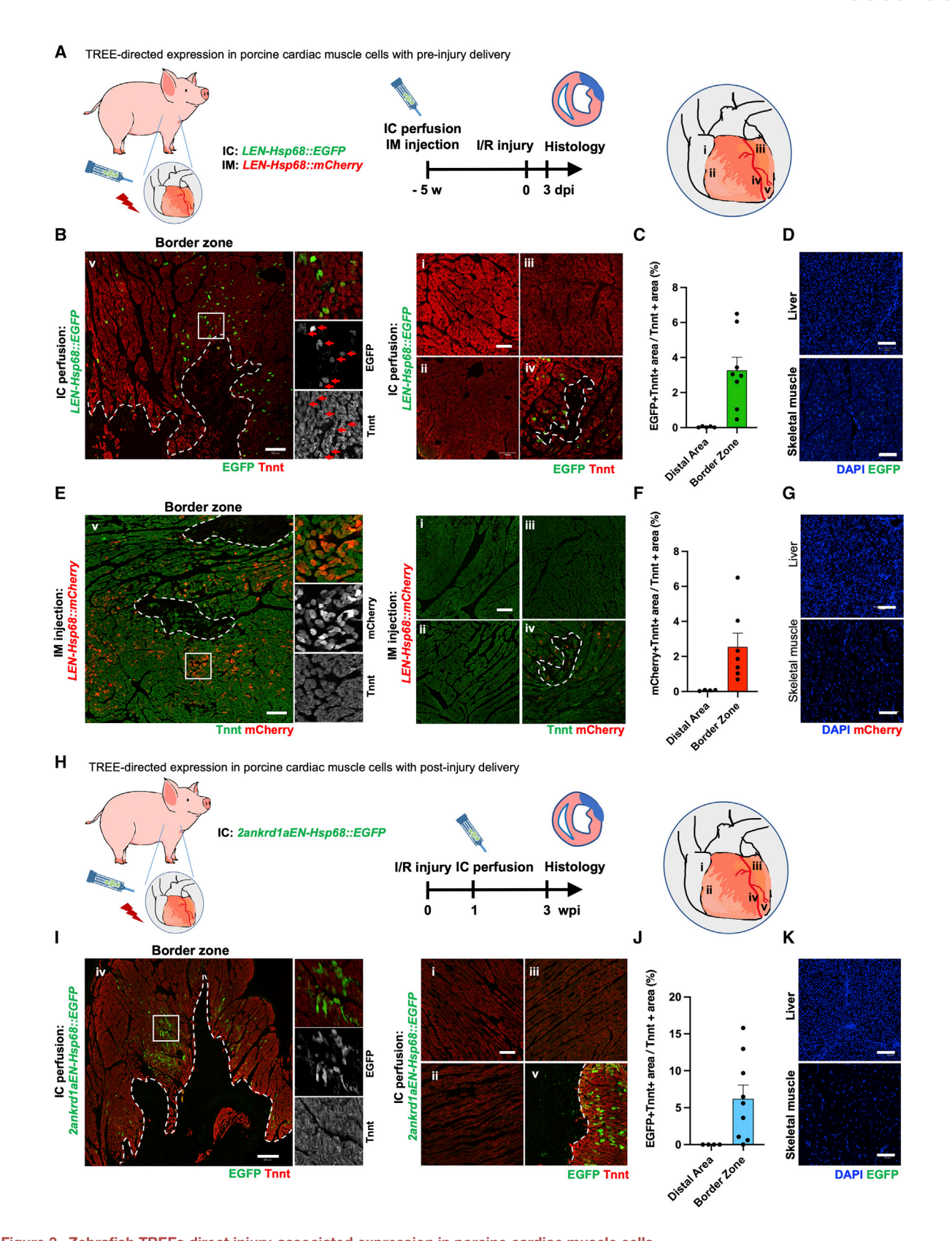


Figure 3. Zebrafish TREEs direct injury-associated expression in porcine cardiac muscle cells (A) Experimental design in (B)–(G), in which pigs are transduced by intracoronary (IC) perfusion or 10–15 intramyocardial (IM) injections throughout the ventricles, prior to ischemia/reperfusion injury (I/R). Regions of the ventricle sampled for histology are indicated by (i)–(v). n = 1.

Resource



(REN, LEN, and 2ankdr1aEN) induced reporter expression in injured mice (Figure 2B), with EGFP expression negligible in sham-injured or uninjured hearts (Figures 2B, S2B, and S2C; Table S1). Reporter-gene expression was detectable in the injury border zone as early as 3 dpi, maintained for at least 2 weeks, and weak or undetectable by 50-70 dpi, whereas little or no expression was detectable in distal areas (Figure 2B).

TREE-directed expression domains were predominantly detected in cells also expressing the CM marker troponin T (Figures 2C and S2D), whereas little or no EGFP expression was detectable in CD31⁺ endothelium, CD68⁺ macrophages, or Vimentin+ fibroblasts (Figure S2E). This is consistent with the tropism of AAV9 for heart muscle cells in cardiac tissue.³⁵ Quantification of myocardial EGFP fluorescence in several animals at different time points indicated that the efficacy of TREE-directed expression was variable but consistently much more prevalent in the border zone than in distal areas (Figure S2D). To assess off-target expression, we examined livers of mice after MI injury, given the expected heavy viral load in this tissue. Whereas histology revealed ~24% of hepatocytes displaying detectable REN-directed EGFP expression, only \sim 6% and \sim 2% of hepatocytes displayed *LEN*- or *2ankdr1aEN*based EGFP expression, respectively (Figure S2F). LEN, REN, and 2ankdr1aEN also directed EGFP expression when coupled with a murine minimal c-fos promoter, although with lower efficiency than with the Hsp68 promoter (Figure S2G). We also assessed the ability of smaller TREE fragments to direct gene expression following cardiac injury, finding the fragments we tested to be less consistent or robust than fulllength TREEs (Figures S3A and S3B). These findings indicate that zebrafish TREEs can be employed in AAV-based vectors to rapidly direct transient gene expression to cardiac injury sites.

To test whether these same enhancers could direct gene expression if delivered by AAV after MI, we injured adult mice and systemically delivered AAV9-harboring TREE constructs at different times after injury (Figures 2E and S3C-S3E). Notably, we found that LEN, REN, and 2ankrd1aEN directed EGFP fluorescence in myocardium from AAVs when delivered 1 day after MI (Figure 2E). Whereas LEN and REN directed little or no EGFP when AAVs were delivered 7, 30, or 50 days post MI, 2ankrd1aEN could still direct strong EGFP expression when delivered at 7 and 30 days post MI (Figures S3C-S3E). Thus, while different zebrafish TREEs have distinct expression capabilities, they are able to target gene expression to MI border zones whether delivered systemically on AAV vectors before or after the injury, a finding that is relevant to potential therapeutic regimens.

Zebrafish TREEs target gene expression to porcine cardiac injuries

To test in vivo recognition in large mammals, we introduced LEN-Hsp68::mCherry AAV9 by multiple (10-15) direct intramyocardial (IM) injections broadly throughout the heart, as well as LEN-Hsp68::EGFP AAV9 by intracoronary (IC) perfusion, to young Yorkshire breed swine 5 weeks before an ischemia/reperfusion (I/R) injury (Figure 3A). Peripheral intravenous delivery was not used because of the large amounts of virus needed to achieve broad transduction in pigs. Many regions of cardiac tissue within and remote to the injury site were collected for expression analysis at 3 dpi. We detected expression of both LEN-based reporter genes preferentially in injury border-zone tissue and targeting a relatively low percentage (~2%-3%) of borderzone CMs as assessed by histological snapshots, indicating efficacy whether delivered IM or through coronary vasculature (Figures 3B, 3C, 3E, and 3F). EGFP or mCherry expression was negligible in liver and skeletal muscle of these animals, indicating effective tissue targeting (Figures 3D and 3G).

To examine the ability of TREEs to direct expression when delivered 1 week after injury, pigs were given I/R injuries and 2ankrd1aEN-Hsp68::EGFP AAV9, selected for its robust activity when delivered post I/R in mice, was introduced by IC injection (Figure 3H). IC was chosen as a less invasive and potentially less injurious protocol than IM. Under this regimen, the 2ankrd1aEN-directed EGFP reporter gene was expressed selectively in the injury border zone in \sim 5% of CMs, assessed at 2 weeks after transduction (Figures 3I and 3J), with negligible expression in areas distant from injured or at-risk myocardium, in liver, or in skeletal muscle (Figures 3J and 3K). These findings indicate that zebrafish TREEs have broad cross-species effects and are capable of targeting gene expression to cardiac injury sites in large mammals.

⁽B) Section images of hearts after I/R injury, from pig transduced preinjury with AAV9 harboring a zebrafish TREE LEN, an Hsp68 minimal promoter, and an EGFP (IC perfusion) cassette. Fluorescence is induced by injury and restricted to CMs near the ischemic injury. White dashed lines indicate injured area. Scale bars: 200 μ m (left) and 100 μ m (right).

⁽C) Quantified EGFP expression of injured hearts from pig in (B). Graph indicates mean ± SEM.

⁽D) Section images of liver and skeletal muscle after I/R injury, from pig transduced as above. Fluorescence is negligible in liver and skeletal muscle. Scale

⁽E) Section images of hearts after I/R injury, from pig transduced preinjury with AAV9 harboring a zebrafish TREE LEN, an Hsp68 minimal promoter, and an mCherry (IM injection) cassette. Fluorescence is induced by injury and restricted to CMs near the MI. White dashed lines indicate injured area. Scale bars: 200 μm (left) and 100 μm (right).

⁽F) Quantified mCherry expression of injured hearts from pig in (E). Graph indicates mean ± SEM.

⁽G) Section images of liver and skeletal muscle after I/R injury, from pig transduced by IM injection as above. Fluorescence is negligible in liver and skeletal muscle. Scale bars, 100 um.

⁽H) Experimental design in (I)–(K), in which pigs are transduced by intracoronary (IC) perfusion 1 week post I/R injury. Regions of the ventricle sampled for histology are indicated by (i)–(v). n = 1.

⁽I) Section images of hearts after I/R injury, from pig transduced postinjury with AAV9 harboring a zebrafish TREE 2ankrd1aEN, an Hsp68 minimal promoter, and an EGFP cassette. Fluorescence is induced by injury and restricted to CMs near the MI. Scale bars, 200 μm (left) and 100 μm (right).

⁽J) Quantified EGFP expression of injured hearts from pig in (I). Graph indicates mean ± SEM.

⁽K) Section images of liver and skeletal muscle after I/R injury, from pig transduced as above. Fluorescence is negligible in liver and skeletal muscle. White dashed lines indicate injured area. Scale bars, 100 μm .



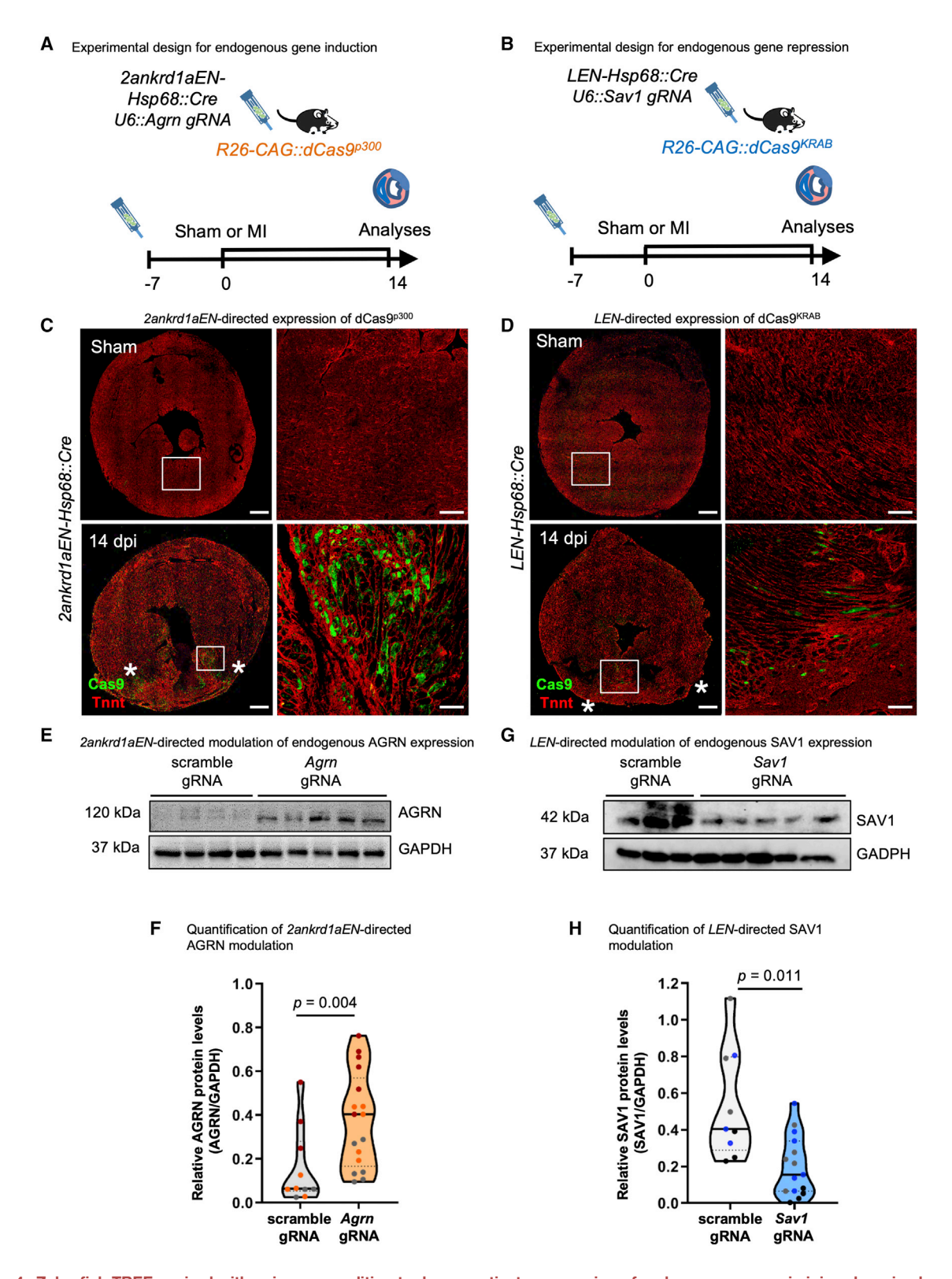


Figure 4. Zebrafish TREEs paired with epigenome editing tools can activate expression of endogenous genes in injured murine hearts (A and B) Experimental design for in vivo modulation of endogenous gene expression, involving transgenic mice enabling Cre-based expression of dCas9-based epigenome editors and AAVs containing TREE-controlled Cre and a U6-gRNA expression cassette.

(legend continued on next page)

Resource



CRISPR-TREE systems modulate endogenous gene expression in myocardial injury sites of mice

The ability to perturb endogenous gene expression in vivo is a powerful tool with potential applications to regeneration. 36-39 To determine whether zebrafish TREEs could promote injuryassociated epigenome editing in mouse heart, we employed mouse lines carrying a CAG promoter upstream of a loxPstop-loxP (LSL) cassette, followed by dCas9 fused either to the p300 core acetyltransferase domain or Krüppel associated box (KRAB) domain coding sequences (Rosa26:LSL-dCas9^{p300} and Rosa26:LSL-dCas9^{KRAB}) (Figure S4A).³⁶ These dCas9 fusion proteins activate or repress target gene expression, respectively, if an appropriate guide RNA (gRNA) is present. 40-42 To evaluate the efficacy of the dCas9^{p300} and dCas9^{KRAB} lines in the adult mouse heart, we injected mice with AAV9-expressing Cre recombinase under the control of a cytomegalovirus (CMV) promoter by tail vein injection. Injected mice displayed induced dCas9^{p300} and dCas9^{KRAB} expression in the ventricle 2 weeks after injection, with variability in levels among individual mice, as assessed by western blotting and immunofluorescence (Figures S4B-S4E). To test whether endogenous gene expression could be manipulated, we targeted two genes implicated in CM biology, Agrin (Agrn) and Salvador (Sav1).31,43,44 We designed 4 gRNAs targeting the promoter region of Agrn and 8 gRNAs targeting the promoter region of Sav1, incorporated them individually downstream of a U6 promoter into AAV genome constructs together with a CMV::Cre cassette, and transduced dCas9^{p300} or dCas9^{KRAB} mice. 2 weeks after the introduction of Agrn gRNAs into dCas9^{p300} mice, we observed an average \sim 60% increase in Agrn mRNA levels and an average \sim 54% increase in AGRN protein levels using one of the four gRNAs tested, again with variability among animals (Figures S4F-S4I). In dCas9KRAB mice injected with Sav1 gRNAs, we observed an average ${\sim}85\%$ reduction of Sav1 mRNA levels and an average $\sim\!56\%$ decrease in SAV1 protein levels with one of the eight gRNAs tested at 2 weeks after AAV injection (Figures S4J-S4M).

To assess whether zebrafish TREEs could direct dCas9^{p300} and dCas9KRAB activities, we generated AAV9 constructs harboring either LEN or 2ankd1aEN upstream of a Hsp68::Cre cassette, using two different TREEs to test generalizability. We injected dCas9^{p300} or dCas9^{KRAB} mice with AAVs, performed MI injuries, and analyzed hearts by immunofluorescence at 14 dpi (Figures 4A and 4B). In these experiments, dCas9^{p300} or dCas9KRAB expression was preferentially induced near and within the injured myocardium (Figures 4C and 4D). Next, we injected AAVs carrying 2ankd1aEN-Hsp68::Cre; U6::Agrn gRNA or LEN-Hsp68::Cre; U6::Sav1 gRNA into dCas9p300 and dCas9KRAB mice, respectively, induced MI, and harvested hearts at 14 dpi. AGRN protein levels were ~41% higher on average in dCas9^{p300} ventricles of mice transduced with 2ankd1aEN-Hsp68::Cre; U6::Agrn gRNA AAV compared with mice treated with nontargeting gRNAs (Figures 4E and 4F). Conversely, SAV1 protein levels were ~62% lower on average in hearts of dCas9KRAB mice transduced with LEN-Hsp68::Cre; U6::Sav1 gRNA AAV compared with controls (Figures 4G and 4H). These experiments provide proof-of-principle evidence that TREEs can be incorporated into viral vectors to increase or reduce the expression of endogenous genes upon injury using CRISPRbased epigenome editing.

TREE-based gene delivery elevates CM cycling after ischemic heart injury

Proliferation of pre-existing CMs is the primary cellular source of new muscle during cardiac regeneration in zebrafish and neonatal mice. 22,23,45 Recent studies demonstrate that suppression of the Hippo pathway or overexpression of the active form of Yap transcriptional coactivator elevates CM division in either developing or adult mice. 28,31,44,46-50 Multiple direct cardiac injections of AAVs expressing a YAP with an activating mutation into murine MI injury sites was reported to increase indicators of CM cycling and organ function. 49 A different study assessed effects of induced, cardiac-wide expression of a YAP cassette with additional mutations in transgenic mice. This study reported sharply induced cycling in CMs and non-CMs with animals dying within days of induced expression mortality associated with cardiac muscle growth and occlusion of ventricular chambers.²⁸ We postulated that direction of mutated YAP by a TREE would preferentially direct cardiogenic events to the border zone with injury-associated temporal dynamics.

To determine the effects of TREE-directed YAP activity in adult mice, we introduced LEN-Hsp68::HA-YAP5SA or control LEN-Hsp68::EGFP AAVs by tail vein injection, ligated the LCA 1 week later, and collected hearts at 3, 14, or 35 dpi (Figure 5A). LEN was selected based on our having the most experience with it among TREEs as well as its low hepatic expression, and a YAP5SA with mutations in 5 inhibitory phosphorylation sites was used.⁵¹ As predicted, LEN-based YAP5SA expression was observed selectively in the border zone at 3 and 14 dpi, with immunofluorescence revealing nuclear accumulation of YAP, whereas little to no expression was observed at 35 dpi

⁽C and D) Section images from ventricle of Rosa26;:LSL-dCas9^{c300} (in C) or Rosa26;;LSL-dCas9^{KRAB} (D) mice injected with AAV9 carrying a zebrafish TREE, an Hsp68 minimal promoter, and a Cre recombinase. Cas9 protein (green) is detected in CMs (red, Tnnt) near the injury site (asterisks). n = 3. Scale bars, 500 and 100 um (magnified areas).

⁽E) Representative western blot images of AGRN and GAPDH protein levels in hearts of Rosa26:;LSL-dCas9^{p300} mice injected with AAV9-2ankrd1aEN-Hsp68:;Cre containing a control nontargeting gRNA or Agrn gRNA and sacrificed at 14 dpi. Each lane represents sampling of one animal.

⁽F) Quantification of AGRN protein levels from 3 independent experiments; all samples are included in the graph and color coded for each experiment. Each point represents one mouse. Mann-Whitney rank-sum test; n = 10 for scramble gRNAs and n = 17 for Agrn gRNAs. Solid line on violin plot indicates the median.

⁽G) Representative western blot images of SAV1 and GAPDH protein levels from hearts of Rosa26:LSL-dCas9^{KRAB} mice injected with AAV9-LEN-Hsp68:Cre containing a scramble or Sav1 gRNA and sacrificed at 14 dpi.

⁽H) Quantification of SAV1 protein levels from three independent experiments; all samples are included in the graph and color coded for each experiment. Each point represents one mouse. Unpaired t test with Welch's correction; n = 9 for control nontargeting gRNAs and n = 15 for Sav1 gRNAs. Solid line on violin plot indicates the median.



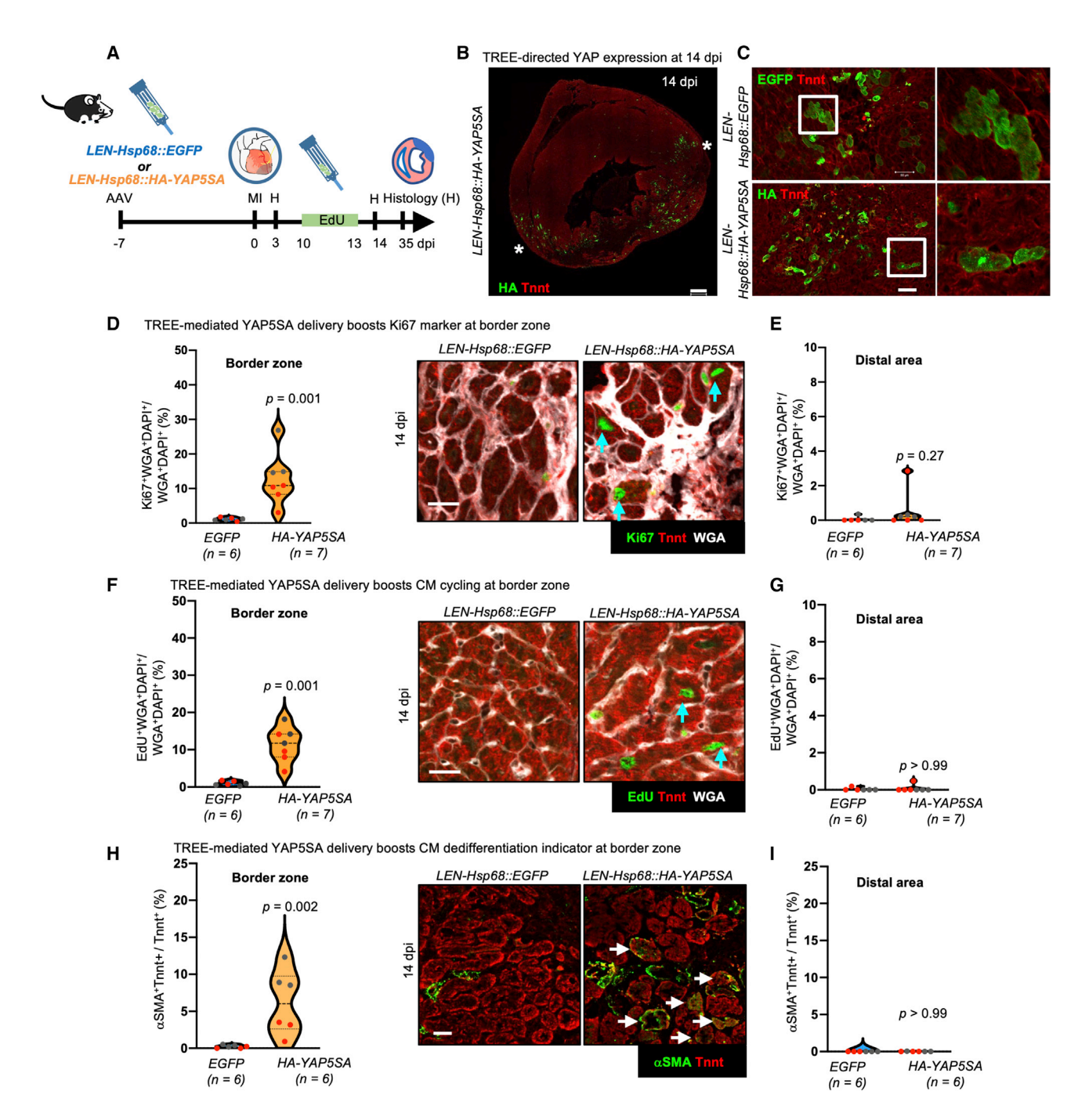


Figure 5. TREE-mediated YAP5SA delivery boosts CM cycling

(A) Experimental design in (B)-(I). An AAV with LEN directing EGFP or a YAP5SA cassette is delivered 1 week before myocardial infarction. (B and C) Section images of 14 dpi hearts from adult mice transduced preinjury with AAV9 harboring LEN-Hsp68::EGFP or LEN-Hsp68::HA-YAP5SA. EGFP or HA is induced at the site of injury (asterisks) in LEN-Hsp68::EGFP or LEN-Hsp68::HA-YAP5SA hearts, respectively. High-magnification view of box in left. Scale bars, $500 \mu m$ (B) and $50 \mu m$ (C).

(D) (Left) Quantified CM Ki67 indices in the border zone. Mann-Whitney test. (Right) Section images of border zone stained for the CM marker Tnnt (red), WGA (white), and cycling marker Ki67 (green). Arrows indicate Ki67* CM nuclei. Scale bars, 20 µm. Lines on violin plots indicate the median and quartiles.

(E) Quantified CM Ki67 indices in distal myocardium. Mann-Whitney test. Lines on violin plots indicate the median and quartiles.

(F) (Left) Quantified CM EdU incorporation indices in the border zone. Mann-Whitney test. (Right) Section images of border zone stained for CM marker Tnnt (red), wheat germ agglutinin (WGA; white), and EdU (green). Arrows indicate EdU+ CM nuclei. Scale bars, 20 µm. Lines on violin plots indicate the median and quartiles. (G) Quantified CM EdU incorporation indices in distal myocardium. Mann-Whitney test. Lines on violin plots indicate the median and quartiles.

Resource



(Figures 5B, 5C, S5A, and S5C). Notably, LEN-Hsp68::HA-YAP5SA-transduced mice displayed a visible and selective increase in the number of cells positive for Ki67, a marker of cycling cells, in the border zone at 14 dpi, compared with control LEN-Hsp68::EGFP hearts (Figures S5D and S5E), whereas no obvious differences were observed at 3 dpi (Figure S5B). Quantification of CM cycling indices in border zones of LEN-Hsp68::HA-YAP5SA-infected animals compared with LEN-Hsp68::EGFP controls at 14 dpi revealed increases of 11.4% versus 1.0% in EdU incorporation indices, and 12.7% versus 1.1% in CM nuclear Ki67 indices (Figures 5D, 5F, and S5F). By contrast, no differences in CM-cycling indicators were observed distant from injuries (Figures 5E, 5G, and S5F), nor in livers (Figure S5L). Cell-cycle markers were not tightly associated with YAP5SA positivity, which showed less nuclear accumulation at 14 dpi as compared with 3 dpi (Figures 5B and S5A). Cycling events in YAP5SA-negative CMs might reflect responses in cells that had expressed YAP5SA before 14 dpi, and/or effects of YAP5SA-expressing cells on neighboring cells. This observation and analogous possible explanations were also provided in the aforementioned Monroe et al.²⁸ study.

In addition to these indicators of cell cycling, we observed a similar increase in the percentage of CMs positive for smooth muscle α -actin (α SMA), a marker of CM dedifferentiation,³² selectively in 14 dpi border zones of LEN-Hsp68::HA-YAP5SAtransduced animals (6.2% versus 0.2% in controls) (Figures 5H, 5I, S5G, and S5H). Cells expressing αSMA were identified as CMs by sarcomere presence and co-expression of Tnnt and as not expressing the fibroblast marker Vimentin (Figures S5I and S5J). In addition, we assessed off-target expression in livers of mice after MI injury, given the expected heavy viral load in this tissue. LEN-Hsp68::HA-YAP5SA-transduced mice displayed limited HA expression in hepatocytes at 35 dpi, and no hepatic Ki67 expression difference that might result from possible hepatic YAP5SA presence was observed at 35 dpi compared with control LEN-Hsp68::EGFP livers (Figures S5K and S5L).

TREE-based gene delivery improves indicators of cardiac function in mice

To examine whether cellular indicators of regeneration were associated with changes in overall cardiac function, we induced myocardial ischemia in mice 15 days after systemic administration of either LEN-Hsp68::HA-YAP5SA or LEN-Hsp68::EGFP AAVs, allowing reperfusion after a 1-h ligation period. We performed echocardiography prior to AAV injection, again prior to injury, and then weekly over a period of 6 weeks (Figure 6A). Animal survival was similar in each group (Figure S6B), as was the portion of animals showing evidence of injury at 3 days post I/R (dpi) by echocardiography (>10% relative reduction in ejection fraction [EF] observed in 8 of 13 surviving YAP5SA animals; 7 of 12 EGFP). The average reduction in EF at 3 dpi was comparable among these animals, indicating a similar initial injury, also supported by measurements of infarcted areas by tetrazolium staining (Figures 6B, S6A, and S6C). By following the performance of these animals individually, our analysis indicated that mice transduced with LEN-Hsp68::HA-YAP5SA displayed higher EFs and fractional shortening (FS) on average beyond 3 dpi than LEN-Hsp68::EGFP-transduced mice (Figures 6B, 6C, 6J, S6C, S6D, and S6L; Table S2). At the experimental endpoint of 42 dpi, EFs in LEN-Hsp68::EGFPtransduced mice had dropped to 36.01% from the 3 dpi value of 40.00%, and those in LEN-Hsp68::HA-YAP5SA-transduced mice had risen to 48.42% from 41.23% (sham EF at 42 dpi, 57.37%) (Figure S6C). Certain left-ventricular-wall thickness indicators were increased in LEN-Hsp68::HA-YAP5SAtransduced mice, and indicators of chamber dilation were reduced, compared with LEN-Hsp68::EGFP-transduced mice (Figures 6D-6J and S6E-S6L; Table S2). Interestingly, these overall functional improvements were not accompanied by differences in fibrosis as measured in cardiac sections (Figures 6K, S6M, and S6N). Gross similarities in scarring might mask underlying cellular or subcellular differences in myocardial or fibrotic tissue that impact function; additionally, human patients can have a considerable scar burden without displaying significant left ventricular dysfunction.⁵²

To test for effects of TREE-delivered YAP5SA in a more therapeutic context, we administered LEN-Hsp68::HA-YAP5SA to mice 1 day after LCA ligation and again allowed reperfusion after a 1-h ligation period. We performed echocardiography prior to injury and then weekly over the following 6 weeks (Figure 6A). Mice transduced with LEN-Hsp68::HA-YAP5SA in these experiments experienced a comparable reduction in EF by 3 dpi as other groups (Figures 6B and S6C). Subsequently, animals displayed trending improvements in EF and FS, with EF increasing from 42.21% at 3 dpi to 50.91% by 42 dpi (Figures 6B, 6C, 6J, S6C, S6D, and S6L; Table S2). As with animals in the LEN-Hsp68::HA-YAP5SA pretreatment group, we observed indications of increased wall thickening and decreased chamber dilation, assessed as tracked individual performance after injury or at the endpoint of 42 dpi (Figures 6D-6J and S6E-S6L; Table S2). Finally, histology revealed obvious scars in each injured ventricle at 42 dpi, with measurably similar fibrosis indices as in the two parallel groups (Figures 6K, S6M, and S6N). In total, our findings indicate that zebrafish TREEs present in systemically delivered viral vectors can guide expression of known proregenerative factors to injury sites, selectively boosting CM-regeneration indicators and leading to measurable improvements in cardiac function.

DISCUSSION

Major challenges to molecular therapies include not only identifying agents and effectors but also targeting interventions for specificity and safety. Implanted devices can conceivably deliver a compound to a defined area, using machine and human

(H) (Left) Quantified CM dedifferentiation indices in the border zone. Mann-Whitney test. (Right) Section images of border zone stained for CM marker Tnnt (red), and dedifferentiation marker αSMA (green). αSMA marks vascular smooth muscle and immature CMs, and CM αSMA staining is greater in the border zones of experimental animals. Arrows indicate αSMA+ CMs. Scale bars, 50 μm. Lines on violin plots indicate the median and quartiles.

(I) Quantified CM dedifferentiation indices in distal myocardium. Mann-Whitney test. Values in (D)-(I) are from 2 independent experiments. Each point represents one mouse and each color represent samples of an independent experiment. Lines on violin plots indicate the median and quartiles.

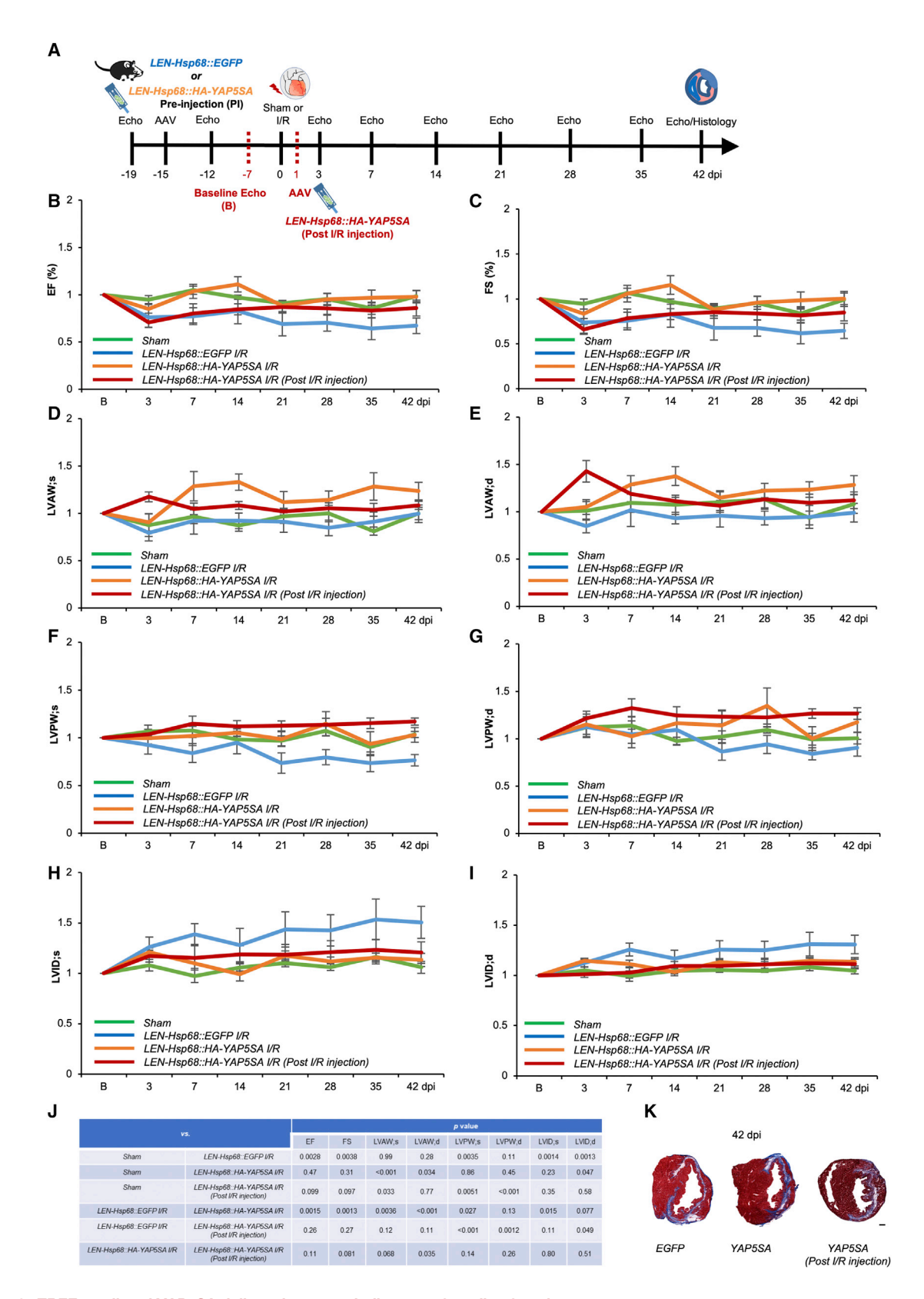


Figure 6. TREE-mediated YAP5SA delivery improves indicators of cardiac function (A) Experimental design for AAV introduction, I/R injury, echocardiographic monitoring, and collection for histology.

Resource



monitoring to control dosing.⁵³ Gene therapy has advantages over these technologies, which include persistent, DNA-powered expression, some extent of tissue targeting, and modularity for applications like gene overexpression or gene editing. Yet, the abilities to limit gene expression to subregions of tissue, and to establish a temporal window of expression, are priority goals for gene therapy that have not been met. As we report here, TREE-regulatory elements contain natural instructions within short sequences to monitor injury and dynamically control amounts, range, and duration of dosing in mammalian injury contexts. TREE instructions can be delivered noninvasively through vasculature, simplifying delivery methods that are currently problematic for tissues like the heart. Different TREEs have distinct activity profiles, which might enable tailoring to an individual patient, and their features allow for reactivation of an expression response in recurrent disease events like successive MIs. Incorporation of TREEs into nonintegrating AAV vectors could help to form and shape concepts of gene therapy with increased safety.

The most ambitious toolset of regenerative medicine is molecular-that is, compounds or gene vectors that boost the latent regenerative capacity of injured human tissues without the addition of cells, parts, or pieces. Mammals likely possess all gene products required to regenerate an injured heart, crushed spinal cord connections, or amputated limbs. Indeed, neonatal mammals can regenerate after major cardiac or spinal cord injury, 23,54 and humans can regenerate lost digit tips.55-57 However, mammals lack or gradually lose the competency to deliver and/or receive instructions that strategically modulate those gene products for regeneration. One facet of this competency likely exists in the form of gene-regulatory elements that remain or become accessible to execute instructions in contexts of elevated regenerative capacity, as displayed by zebrafish. Here, we find that even in situations of limited regenerative capacity, the transcriptional machinery of small and large adult mammals can recognize and be instructed by TREE sequences from zebrafish, present in transgenes or viral vectors. In these contexts, we infer that sequences within TREEs responsive to the injury component of regeneration, rather than components like tissue morphogenesis, are interpreted. This recognition is ostensibly based on functional conservation of cis-regulatory elements rather than high-sequence conservation. 19 Critical insights can emerge from identification of injury-related stimuli and specific factors that activate and bind TREEs, which can

be approached with screens or proteomics in zebrafish or mammals. Analysis of transcription-factor-binding sites within LEN, REN, and 2ankrd1a identified a subset of shared, predicted binding motifs as candidates to engage with these signals (Figure S6O). Deconstruction of TREE sequences into signals and stimuli has the potential to broaden their applications, possibly enabling spatiotemporal control from gene-therapy vectors by drugs that can mimic a triggering injury.

Limitations of the study

Experiments reported here advance a proof-of-principle genetherapy strategy, and it is important to acknowledge limitations of the study. Perhaps foremost, the expression responses guided by TREEs in response to cardiac injury can be highly variable when assessed in a pool of animals by histological analysis. Many factors likely contribute to this, including the underpublicized variability in the extent of muscle loss after MI or I/R in mouse models. Differing transduction efficiency of AAVs among animals brings additional variability. We also expect that individual cells in a tissue field adjacent to the injury each have unique thresholds for activation that are determined by factors like transcriptome noise and distance from the injury. Heterogeneity in factors like these likely also affect temporal windows of expression, such that in a tissue field there may be some cells that have not engaged TREE-directed expression, some recently engaged, some that have had TREE-directed expression for a few days and are in the process of diminution, and some that have already terminated expression.

Many components of the technology we describe can be modified for efficacy and safety. Panels of regulatory elements from diverse species and tissues, including those mined from mouse and human genomes, can be identified and optimized for sequence length and expression features like cell-type specificity, strength, and temporal dynamics. Payloads need not be mitogens but could include agents for vascularization, innervation, cell survival, inflammation, scarring, or genetic correction. which could be provided combinatorically in a single vector or multiple vectors harboring one or more enhancer regulatory sequences. Animals transduced with TREE constructs should be monitored for extended periods of time, and with models of repeated minor or major injuries. Finally, a major objective must be the elimination of off-target gene expression. Such activity might be difficult to eliminate entirely, and even low levels in remote organs could be detrimental. Further honing

(B and C) Ejection fractions (EFs) and fractional shortening (FS) were calculated pre- and post-I/R. Shown are normalized mean ± SEM for animals from each group that displayed a loss in EF of relative 10% or more at 3 dpi as compared with the previous measurement at baseline prior to injury.

(D and E) Left ventricular anterior wall dimensions during systole (LVAW;s) (D) and diastole (LVAW;d) (E) were calculated pre- and post-I/R. Shown are normalized mean ± SEM for animals described in (A).

(F and G) Left ventricular posterior wall dimensions during systole (LVPW;s) (F) and diastole (LVPW;d) (G) were calculated pre- and post-I/R. Shown are normalized mean ± SEM for animals described in (A).

(H and I) Left ventricular internal diameter end systole (LVID;s) (H) and diastole (LVID;d) (I) were calculated pre- and post-I/R. Shown are normalized mean ± SEM for animals described in (A).

(J) Wald's tests were used for statistical comparisons of functional indicators among groups from 7 to 42 dpi, which preserved individual animal performance over time. p values for the Wald's tests are shown in the table. Graphs and statistical analysis of pooled actual (rather than normalized) values are shown in

(K) Transverse section images from hearts at 42 days post-I/R, stained by Masson's trichrome to highlight collagen (blue). One representative section from a LEN-Hsp68::EGFP, a LEN-Hsp68::HA-YAP5SA heart, and a LEN-Hsp68::HA-YAP5SA post I/R injection heart are shown. n = 8, 7, 8, and 7-8 for sham, LEN-Hsp68::EGFP, LEN-Hsp68::HA-YAP5SA, and LEN-Hsp68::HA-YAP5SA post I/R injection, respectively (one animal died between 36 and 42 dpi in the LEN-Hsp68::HA-YAP5SA post I/R injection group). Scale bars, 500 μm. Representative sections from each heart are shown in Figure S6.





the cell-type specificity of TREEs and using existing or emerging tissue/cell-selective AAV capsids can mitigate this and provide additional levels of specificity.

STAR*METHODS

Detailed methods are provided in the online version of this paper and include the following:

- KEY RESOURCES TABLE
- RESOURCE AVAILABILITY
 - Lead contact
 - Materials availability
 - Data and code availability
- EXPERIMENTAL MODEL AND SUBJECT DETAILS
 - Zebrafish
 - Mice
- METHOD DETAILS
 - Generation of TREE-Hsp68::LacZ transgenic mice
 - Ligation of the left coronary artery
 - Ischemia/reperfusion injury
 - Skeletal muscle injury
 - Tibial fracture
 - Digit amputation
 - O AAV plasmid construction and virus production
 - O Histology and imaging in zebrafish
 - Cardiac function assessed by echocardiography
 - O Histology and imaging in mice
 - RNA isolation and qRT-PCR
 - O Protein isolation and western blotting
 - Large animal studies
- QUANTIFICATION AND STATISTICAL ANALYSIS

SUPPLEMENTAL INFORMATION

Supplemental information can be found online at https://doi.org/10.1016/j.stem.2022.11.012.

ACKNOWLEDGMENTS

We thank Duke DLAR staff for mouse and swine care; Duke Cardiovascular Physiology Core, J. Stowell, and S. Degan for performing mouse MI surgeries; B. Varelas for plasmid; C. Bryant and N. Lee for technical help; Duke Zebrafish Core for zebrafish care; and F. Sun and M. Pronobis for comments on the manuscript. R.Y. was supported by an American Heart Association (AHA) postdoctoral fellowship (17POST33660087). V.C. was supported by Early (P2GEP3_175016) and Advanced (P400PM_186709) Postdoc Mobility fellowships from the Swiss National Science Foundation. S.D. was supported by predoctoral fellowships from AHA (903369) and NIH (F31 HL162460). J.K. acknowledges support from National Institutes of Health (R01 HL151522) and AHA (AHA16SDG30020001). J.A.G. acknowledges support from AHA (AHA117SDG33660922). G.S.B. acknowledges support from the Claude D. Pepper Older Americans Independence Center Pilot Award (P30AG028716) and NIH (R21 AG067245). R.K. acknowledges support from Transforming Duke Health (TDH) and NIH (R01 HL157277). C.A.G. acknowledges support from NIH (U01Al146356, UM1HG013053, RM1HG011123, R33DA041878), National Science Foundation (EFMA-1830957), the Duke-Coulter Translational Partnership, and an Allen Distinguished Investigator Award. N.B. acknowledges support from NIH (U01 HL134764 and R01 HL126524), TDH, and Fondation Leducq. B.L.B. acknowledges support from NIH (R01 HL146366 and R01 DK119621). K.D.P. acknowledges support from NIH (R35 HL150713 and R01 HL136182), AHA, TDH, and Fondation Leducq.

AUTHOR CONTRIBUTIONS

Conceptualization, R.Y., V.C., and K.D.P.; methodology, R.Y., V.C., T.S., D.E.B., A.A., E.T., J.D.M., N.B., B.L.B., and K.D.P.; formal analysis, R.Y., V.C., K.A.O., Z.P., S.D., D.W.W., P.D., J.O., R.K., and K.D.P.; investigation, R.Y., V.C., K.A.O., Z.P., S.D., D.W.W., A.V., M.A.M., G.D., M.B., M.A.S., A.J.Y., A.S., D.C.W., G.S.B., and A.R.W.; writing – original draft, R.Y. and V.C.; writing – review and editing, R.Y., V.C., and K.D.P.; resources and funding acquisition, M.P.G., J.K., J.A.G., R.K., A.A., E.T., C.A.G., J.D.M., N.B., B.L.B., and K.D.P. All authors read and commented on or edited the manuscript.

DECLARATION OF INTERESTS

R.Y., J.K., J.A.G., V.C., and K.D.P. are listed as inventors on a patent application filed by Duke University on methods for enhancing tissue regeneration. C.A.G. is an inventor on patents and patent applications related to epigenome editing, is a co-founder/advisor of Tune Therapeutics and Locus Biosciences, and is an advisor to Sarepta Therapeutics.

Received: February 27, 2022 Revised: October 6, 2022 Accepted: November 15, 2022 Published: December 13, 2022

REFERENCES

- Kuzmin, D.A., Shutova, M.V., Johnston, N.R., Smith, O.P., Fedorin, V.V., Kukushkin, Y.S., van der Loo, J.C.M., and Johnstone, E.C. (2021). The clinical landscape for AAV gene therapies. Nat. Rev. Drug Discov. 20, 173–174. https://doi.org/10.1038/d41573-021-00017-7.
- Samelson-Jones, B.J., and George, L.A. (2022). Adeno-associated virus gene therapy for hemophilia. Annu. Rev. Med. https://doi.org/10.1146/annurev-med-043021-033013.
- Roger, A.L., Sethi, R., Huston, M.L., Scarrow, E., Bao-Dai, J., Lai, E., Biswas, D.D., El Haddad, L., Strickland, L.M., Kishnani, P.S., and ElMallah, M.K. (2022). What's new and what's next for gene therapy in Pompe disease? Expert Opin. Biol. Ther. 22, 1117–1135. https://doi.org/ 10.1080/14712598.2022.2067476.
- Belbellaa, B., Reutenauer, L., Messaddeq, N., Monassier, L., and Puccio, H. (2020). High levels of frataxin overexpression lead to mitochondrial and cardiac toxicity in mouse models. Mol. Ther. Methods Clin. Dev. 19, 120–138. https://doi.org/10.1016/j.omtm.2020.08.018.
- Matagne, V., Borloz, E., Ehinger, Y., Saidi, L., Villard, L., and Roux, J.C. (2021). Severe offtarget effects following intravenous delivery of AAV9-MECP2 in a female mouse model of Rett syndrome. Neurobiol. Dis. 149, 105235. https://doi.org/10.1016/j.nbd.2020.105235.
- Li, C., and Samulski, R.J. (2020). Engineering adeno-associated virus vectors for gene therapy. Nat. Rev. Genet. 21, 255–272. https://doi.org/10.1038/s41576-019-0205-4.
- Wang, B., Li, J., Fu, F.H., Chen, C., Zhu, X., Zhou, L., Jiang, X., and Xiao, X. (2008). Construction and analysis of compact muscle-specific promoters for AAV vectors. Gene Ther. 15, 1489–1499. https://doi.org/10.1038/gt. 2008.104.
- Kügler, S. (2016). Tissue-specific promoters in the CNS. Methods Mol. Biol. 1382, 81–91. https://doi.org/10.1007/978-1-4939-3271-9_6.
- Goldman, J.A., and Poss, K.D. (2020). Gene regulatory programmes of tissue regeneration. Nat. Rev. Genet. 21, 511–525. https://doi.org/10.1038/s41576-020-0239-7.
- Kang, J., Hu, J., Karra, R., Dickson, A.L., Tornini, V.A., Nachtrab, G., Gemberling, M., Goldman, J.A., Black, B.L., and Poss, K.D. (2016). Modulation of tissue repair by regeneration enhancer elements. Nature 532, 201–206. https://doi.org/10.1038/nature17644.
- 11. Harris, R.E., Setiawan, L., Saul, J., and Hariharan, I.K. (2016). Localized epigenetic silencing of a damage-activated WNT enhancer limits

Resource



- regeneration in mature Drosophila imaginal discs. eLife 5, e11588. https://doi.org/10.7554/eLife.11588.
- Vizcaya-Molina, E., Klein, C.C., Serras, F., Mishra, R.K., Guigó, R., and Corominas, M. (2018). Damage-responsive elements in Drosophila regeneration. Genome Res. 28, 1852–1866. https://doi.org/10.1101/gr. 233098.117.
- Harris, R.E., Stinchfield, M.J., Nystrom, S.L., McKay, D.J., and Hariharan, I.K. (2020). Damage-responsive, maturity-silenced enhancers regulate multiple genes that direct regeneration in Drosophila. eLife 9, e58305. https://doi.org/10.7554/eLife.58305.
- Gehrke, A.R., Neverett, E., Luo, Y.-J., Brandt, A., Ricci, L., Hulett, R.E., Gompers, A., Ruby, J.G., Rokhsar, D.S., Reddien, P.W., and Srivastava, M. (2019). Acoel genome reveals the regulatory landscape of wholebody regeneration. Science 363, eaau6173. https://doi.org/10.1126/science.aau6173.
- Guenther, C.A., Wang, Z., Li, E., Tran, M.C., Logan, C.Y., Nusse, R., Pantalena-Filho, L., Yang, G.P., and Kingsley, D.M. (2015). A distinct regulatory region of the Bmp5 locus activates gene expression following adult bone fracture or soft tissue injury. Bone 77, 31–41. https://doi.org/10. 1016/j.bone.2015.04.010.
- Wang, W., Hu, C.K., Zeng, A., Alegre, D., Hu, D., Gotting, K., Ortega Granillo, A., Wang, Y., Robb, S., Schnittker, R., et al. (2020). Changes in regenerationresponsive enhancers shape regenerative capacities in vertebrates. Science 369, eaaz3090. https://doi.org/10.1126/science.aaz3090.
- Thompson, J.D., Ou, J., Lee, N., Shin, K., Cigliola, V., Song, L., Crawford, G.E., Kang, J., and Poss, K.D. (2020). Identification and requirements of enhancers that direct gene expression during zebrafish fin regeneration. Development 147, dev191262. https://doi.org/10.1242/dev.191262.
- Lee, H.J., Hou, Y., Chen, Y., Dailey, Z.Z., Riddihough, A., Jang, H.S., Wang, T., and Johnson, S.L. (2020). Regenerating zebrafish fin epigenome is characterized by stable lineage-specific DNA methylation and dynamic chromatin accessibility. Genome Biol. 21, 52. https://doi.org/10.1186/ s13059-020-1948-0.
- Goldman, J.A., Kuzu, G., Lee, N., Karasik, J., Gemberling, M., Foglia, M.J., Karra, R., Dickson, A.L., Sun, F., Tolstorukov, M.Y., and Poss, K.D. (2017).
 Resolving heart regeneration by replacement histone profiling. Dev. Cell 40, 392–404.e395. https://doi.org/10.1016/j.devcel.2017.01.013.
- Cao, Y., Xia, Y., Balowski, J.J., Ou, J., Song, L., Safi, A., Curtis, T., Crawford, G.E., Poss, K.D., and Cao, J. (2022). Identification of enhancer regulatory elements that direct epicardial gene expression during zebrafish heart regeneration. Development 149, dev200133. https://doi.org/ 10.1242/dev.200133.
- Chen, A., Han, Y., and Poss, K.D. (2021). Regulation of zebrafish fin regeneration by vitamin D signaling. Dev. Dyn. 250, 1330–1339. https://doi.org/10.1002/dvdy.261.
- Kikuchi, K., Holdway, J.E., Werdich, A.A., Anderson, R.M., Fang, Y., Egnaczyk, G.F., Evans, T., Macrae, C.A., Stainier, D.Y., and Poss, K.D. (2010). Primary contribution to zebrafish heart regeneration by gata4(+) cardiomyocytes. Nature 464, 601–605. https://doi.org/10.1038/ nature08804.
- Porrello, E.R., Mahmoud, A.I., Simpson, E., Hill, J.A., Richardson, J.A., Olson, E.N., and Sadek, H.A. (2011). Transient regenerative potential of the neonatal mouse heart. Science 331, 1078–1080. https://doi.org/10. 1126/science.1200708.
- Soonpaa, M.H., Kim, K.K., Pajak, L., Franklin, M., and Field, L.J. (1996).
 Cardiomyocyte DNA synthesis and binucleation during murine development. Am. J. Physiol. 271, H2183–H2189.
- Patterson, M., Barske, L., Van Handel, B., Rau, C.D., Gan, P., Sharma, A., Parikh, S., Denholtz, M., Huang, Y., Yamaguchi, Y., et al. (2017). Frequency of mononuclear diploid cardiomyocytes underlies natural variation in heart regeneration. Nat. Genet. 49, 1346–1353. https://doi.org/10.1038/ng.3929.
- Wang, Z., Cui, M., Shah, A.M., Ye, W., Tan, W., Min, Y.L., Botten, G.A., Shelton, J.M., Liu, N., Bassel-Duby, R., and Olson, E.N. (2019).
 Mechanistic basis of neonatal heart regeneration revealed by transcrip-

- tome and histone modification profiling. Proc. Natl. Acad. Sci. USA *116*, 18455–18465. https://doi.org/10.1073/pnas.1905824116.
- Puente, B.N., Kimura, W., Muralidhar, S.A., Moon, J., Amatruda, J.F., Phelps, K.L., Grinsfelder, D., Rothermel, B.A., Chen, R., Garcia, J.A., et al. (2014). The oxygen-rich postnatal environment induces cardiomyocyte cell-cycle arrest through DNA damage response. Cell *157*, 565–579. https://doi.org/10.1016/j.cell.2014.03.032.
- Monroe, T.O., Hill, M.C., Morikawa, Y., Leach, J.P., Heallen, T., Cao, S., Krijger, P.H.L., de Laat, W., Wehrens, X.H.T., Rodney, G.G., and Martin, J.F. (2019). YAP partially reprograms chromatin accessibility to directly induce adult cardiogenesis in vivo. Dev. Cell 48, 765–779.e7. https://doi. org/10.1016/j.devcel.2019.01.017.
- Chen, Y., Lüttmann, F.F., Schoger, E., Schöler, H.R., Zelarayán, L.C., Kim, K.P., Haigh, J.J., Kim, J., and Braun, T. (2021). Reversible reprogramming of cardiomyocytes to a fetal state drives heart regeneration in mice. Science 373, 1537–1540. https://doi.org/10.1126/science. abg5159.
- Hassink, R.J., Pasumarthi, K.B., Nakajima, H., Rubart, M., Soonpaa, M.H., de la Rivière, A.B., Doevendans, P.A., and Field, L.J. (2008). Cardiomyocyte cell cycle activation improves cardiac function after myocardial infarction. Cardiovasc. Res. 78, 18–25. https://doi.org/10. 1093/cvr/cvm101.
- Leach, J.P., Heallen, T., Zhang, M., Rahmani, M., Morikawa, Y., Hill, M.C., Segura, A., Willerson, J.T., and Martin, J.F. (2017). Hippo pathway deficiency reverses systolic heart failure after infarction. Nature 550, 260–264. https://doi.org/10.1038/nature24045.
- D'Uva, G., Aharonov, A., Lauriola, M., Kain, D., Yahalom-Ronen, Y., Carvalho, S., Weisinger, K., Bassat, E., Rajchman, D., Yifa, O., et al. (2015). ERBB2 triggers mammalian heart regeneration by promoting cardiomyocyte dedifferentiation and proliferation. Nat. Cell Biol. 17, 627–638. https://doi.org/10.1038/ncb3149.
- Mohamed, T.M.A., Ang, Y.S., Radzinsky, E., Zhou, P., Huang, Y., Elfenbein, A., Foley, A., Magnitsky, S., and Srivastava, D. (2018). Regulation of cell cycle to stimulate adult cardiomyocyte proliferation and cardiac regeneration. Cell 173, 104–116. . e112. https://doi.org/10. 1016/j.cell.2018.02.014.
- Eulalio, A., Mano, M., Dal Ferro, M., Zentilin, L., Sinagra, G., Zacchigna, S., and Giacca, M. (2012). Functional screening identifies miRNAs inducing cardiac regeneration. Nature 492, 376–381. https://doi.org/10.1038/ nature11739.
- Inagaki, K., Fuess, S., Storm, T.A., Gibson, G.A., McTiernan, C.F., Kay, M.A., and Nakai, H. (2006). Robust systemic transduction with AAV9 vectors in mice: efficient global cardiac gene transfer superior to that of AAV8. Mol. Ther. 14, 45–53. https://doi.org/10.1016/j.ymthe.2006.03.014.
- Gemberling, M.P., Siklenka, K., Rodriguez, E., Tonn-Eisinger, K.R., Barrera, A., Liu, F., Kantor, A., Li, L., Cigliola, V., Hazlett, M.F., et al. (2021). Transgenic mice for in vivo epigenome editing with CRISPR-based systems. Nat. Methods 18, 965–974. https://doi.org/10.1038/s41592-021-01207-2.
- Liao, H.K., Hatanaka, F., Araoka, T., Reddy, P., Wu, M.Z., Sui, Y., Yamauchi, T., Sakurai, M., O'Keefe, D.D., Núñez-Delicado, E., et al. (2017). In vivo target gene activation via CRISPR/Cas9-mediated transepigenetic modulation. Cell 171, 1495–1507.e15. https://doi.org/10.1016/j.cell.2017.10.025.
- Hsu, M.N., Liao, H.T., Truong, V.A., Huang, K.L., Yu, F.J., Chen, H.H., Nguyen, T.K.N., Makarevich, P., Parfyonova, Y., and Hu, Y.C. (2019). CRISPR-based activation of endogenous neurotrophic genes in adipose stem cell sheets to stimulate peripheral nerve regeneration. Theranostics 9, 6099–6111. https://doi.org/10.7150/thno.36790.
- Nelson, C.E., Wu, Y., Gemberling, M.P., Oliver, M.L., Waller, M.A., Bohning, J.D., Robinson-Hamm, J.N., Bulaklak, K., Castellanos Rivera, R.M., Collier, J.H., et al. (2019). Long-term evaluation of AAV-CRISPR genome editing for Duchenne muscular dystrophy. Nat. Med. 25, 427–432. https://doi.org/10.1038/s41591-019-0344-3.



Cell Stem Cell Resource

- 40. Hilton, I.B., D'Ippolito, A.M., Vockley, C.M., Thakore, P.I., Crawford, G.E., Reddy, T.E., and Gersbach, C.A. (2015). Epigenome editing by a CRISPR-Cas9-based acetyltransferase activates genes from promoters and enhancers. Nat. Biotechnol. 33, 510-517. https://doi.org/10.1038/nbt.3199.
- 41. Gilbert, L.A., Larson, M.H., Morsut, L., Liu, Z., Brar, G.A., Torres, S.E., Stern-Ginossar, N., Brandman, O., Whitehead, E.H., Doudna, J.A., et al. (2013). CRISPR-mediated modular RNA-guided regulation of transcription in eukaryotes. Cell 154, 442-451. https://doi.org/10.1016/j.cell.2013.06.044.
- 42. Thakore, P.I., D'Ippolito, A.M., Song, L., Safi, A., Shivakumar, N.K., Kabadi, A.M., Reddy, T.E., Crawford, G.E., and Gersbach, C.A. (2015). Highly specific epigenome editing by CRISPR-Cas9 repressors for silencing of distal regulatory elements. Nat. Methods 12, 1143-1149. https://doi.org/10.1038/nmeth.3630.
- 43. Bassat, E., Mutlak, Y.E., Genzelinakh, A., Shadrin, I.Y., Baruch Umansky, K., Yifa, O., Kain, D., Rajchman, D., Leach, J., Riabov Bassat, D., et al. (2017). The extracellular matrix protein agrin promotes heart regeneration in mice. Nature 547, 179-184. https://doi.org/10.1038/nature22978.
- 44. Heallen, T., Zhang, M., Wang, J., Bonilla-Claudio, M., Klysik, E., Johnson, R.L., and Martin, J.F. (2011). Hippo pathway inhibits Wnt signaling to restrain cardiomyocyte proliferation and heart size. Science 332, 458-461. https://doi.org/10.1126/science.1199010.
- 45. Poss, K.D., Wilson, L.G., and Keating, M.T. (2002). Heart regeneration in zebrafish. Science 298, 2188-2190.
- 46. Aharonov, A., Shakked, A., Umansky, K.B., Savidor, A., Genzelinakh, A., Kain, D., Lendengolts, D., Revach, O.Y., Morikawa, Y., Dong, J., et al. (2020). ERBB2 drives YAP activation and EMT-like processes during cardiac regeneration. Nat. Cell Biol. 22, 1346-1356. https://doi.org/10.1038/ s41556-020-00588-4.
- 47. Xin, M., Kim, Y., Sutherland, L.B., Murakami, M., Qi, X., McAnally, J., Porrello, E.R., Mahmoud, A.I., Tan, W., Shelton, J.M., et al. (2013). Hippo pathway effector Yap promotes cardiac regeneration. Proc. Natl. Acad. Sci. USA 110, 13839-13844. https://doi.org/10.1073/pnas.1313192110.
- 48. Heallen, T., Morikawa, Y., Leach, J., Tao, G., Willerson, J.T., Johnson, R.L., and Martin, J.F. (2013). Hippo signaling impedes adult heart regeneration. Development 140, 4683-4690. https://doi.org/10.1242/dev.102798.
- 49. Lin, Z., von Gise, A., Zhou, P., Gu, F., Ma, Q., Jiang, J., Yau, A.L., Buck, J.N., Gouin, K.A., van Gorp, P.R., et al. (2014). Cardiac-specific YAP activation improves cardiac function and survival in an experimental murine MI model. Circ. Res. 115, 354-363. https://doi.org/10.1161/CIRCRESAHA.
- 50. Morikawa, Y., Zhang, M., Heallen, T., Leach, J., Tao, G., Xiao, Y., Bai, Y., Li, W., Willerson, J.T., and Martin, J.F. (2015). Actin cytoskeletal remodeling with protrusion formation is essential for heart regeneration in Hippodeficient mice. Sci. Signal. 8, ra41. https://doi.org/10.1126/scisignal.
- 51. Mahoney, J.E., Mori, M., Szymaniak, A.D., Varelas, X., and Cardoso, W.V. (2014). The hippo pathway effector Yap controls patterning and differentiation of airway epithelial progenitors. Dev. Cell 30, 137-150. https://doi. org/10.1016/j.devcel.2014.06.003.
- 52. Klem, I., Klein, M., Khan, M., Yang, E.Y., Nabi, F., Ivanov, A., Bhatti, L., Hayes, B., Graviss, E.A., Nguyen, D.T., et al. (2021). Relationship of LVEF and myocardial scar to long-term mortality risk and mode of death in patients with nonischemic cardiomyopathy. Circulation 143, 1343-1358. https://doi.org/10.1161/CIRCULATIONAHA.120.048477.
- 53. Lansky, A.J., Kereiakes, D.J., Baumbach, A., Windecker, S., Hussain, Y., Pietras, C., Dressler, O., Issever, O., Curtis, M., Bertolet, B., et al. (2021). Novel supreme drug-eluting stents with early synchronized antiproliferative drug delivery to inhibit smooth muscle cell proliferation after drugeluting stents implantation in coronary artery disease: results of the Pioneer III randomized clinical trial. Circulation 143, 2143-2154. https:// doi.org/10.1161/CIRCULATIONAHA.120.052482.
- 54. Li, Y., He, X., Kawaguchi, R., Zhang, Y., Wang, Q., Monavarfeshani, A., Yang, Z., Chen, B., Shi, Z., Meng, H., et al. (2020). Microglia-organized scar-free spinal cord repair in neonatal mice. Nature 587, 613-618. https://doi.org/10.1038/s41586-020-2795-6.

- 55. Lee, L.P., Lau, P.Y., and Chan, C.W. (1995). A simple and efficient treatment for fingertip injuries. J. Hand Surg. Br. 20, 63-71. https://doi.org/ 10.1016/S0266-7681(05)80019-1.
- 56. Vidal, P., and Dickson, M.G. (1993). Regeneration of the distal phalanx. A case report. J. Hand Surg. Br. 18, 230-233. https://doi.org/10.1016/0266-7681(93)90116-w.
- 57. Illingworth, C.M. (1974). Trapped fingers and amputated finger tips in children. J. Pediatr. Surg. 9, 853-858. https://doi.org/10.1016/s0022-3468(74)80220-4.
- 58. Schindelin, J., Arganda-Carreras, I., Frise, E., Kaynig, V., Longair, M., Pietzsch, T., Preibisch, S., Rueden, C., Saalfeld, S., Schmid, B., et al. (2012). Fiji: an open-source platform for biological-image analysis. Nat. Methods 9, 676-682. https://doi.org/10.1038/nmeth.2019.
- 59. Wang, J., Panáková, D., Kikuchi, K., Holdway, J.E., Gemberling, M., Burris, J.S., Singh, S.P., Dickson, A.L., Lin, Y.F., Sabeh, M.K., et al. (2011). The regenerative capacity of zebrafish reverses cardiac failure caused by genetic cardiomyocyte depletion. Development 138, 3421-3430. https://doi.org/10.1242/dev.068601.
- 60. Dodou, E., Xu, S.M., and Black, B.L. (2003). mef2c is activated directly by myogenic basic helix-loop-helix proteins during skeletal muscle development in vivo. Mech. Dev. 120, 1021-1032. https://doi.org/10.1016/s0925-4773(03)00178-3.
- 61. Curcio, A., Noma, T., Naga Prasad, S.V., Wolf, M.J., Lemaire, A., Perrino, C., Mao, L., and Rockman, H.A. (2006). Competitive displacement of phosphoinositide 3-kinase from beta-adrenergic receptor kinase-1 improves postinfarction adverse myocardial remodeling. Am. J. Physiol. Heart Circ. Physiol. 291, H1754-H1760. https://doi.org/10.1152/ajpheart.01199.2005.
- 62. Kaiser, R.A., Liang, Q., Bueno, O., Huang, Y., Lackey, T., Klevitsky, R., Hewett, T.E., and Molkentin, J.D. (2005). Genetic inhibition or activation of JNK1/2 protects the myocardium from ischemia-reperfusion-induced cell death in vivo. J. Biol. Chem. 280, 32602-32608. https://doi.org/10. 1074/jbc.M500684200.
- 63. An, Y., Wang, G., Diao, Y., Long, Y., Fu, X., Weng, M., Zhou, L., Sun, K., Cheung, T.H., Ip, N.Y., et al. (2017). A molecular switch regulating cell fate choice between muscle progenitor cells and brown adipocytes. Dev. Cell 41, 382-391.e5. https://doi.org/10.1016/j.devcel. 2017.04.012.
- 64. Baht, G.S., Silkstone, D., Nadesan, P., Whetstone, H., and Alman, B.A. (2014). Activation of hedgehog signaling during fracture repair enhances osteoblastic-dependent matrix formation. J. Orthop. Res. 32, 581-586. https://doi.org/10.1002/jor.22562.
- 65. Gray, S.J., Foti, S.B., Schwartz, J.W., Bachaboina, L., Taylor-Blake, B., Coleman, J., Ehlers, M.D., Zylka, M.J., McCown, T.J., and Samulski, R.J. (2011). Optimizing promoters for recombinant adeno-associated virus-mediated gene expression in the peripheral and central nervous system using self-complementary vectors. Hum. Gene Ther. 22, 1143-1153. https://doi.org/10.1089/hum.2010.245.
- 66. Liu, H., and Wang, X. (2021). CRISPR-ERA: A webserver for guide RNA design of gene editing and regulation. Methods Mol. Biol. 2189, 65-69. https://doi.org/10.1007/978-1-0716-0822-7_5.
- 67. Uezu, A., Kanak, D.J., Bradshaw, T.W., Soderblom, E.J., Catavero, C.M., Burette, A.C., Weinberg, R.J., and Soderling, S.H. (2016). Identification of an elaborate complex mediating postsynaptic inhibition. Science 353, 1123-1129. https://doi.org/10.1126/science.aag0821.
- 68. Elmore, Z.C., Patrick Havlik, L., Oh, D.K., Anderson, L., Daaboul, G., Devlin, G.W., Vincent, H.A., and Asokan, A. (2021). The membrane associated accessory protein is an adeno-associated viral egress factor. Nat. Commun. 12, 6239. https://doi.org/10.1038/s41467-021-26485-4.
- 69. Kikuchi, K., Holdway, J.E., Major, R.J., Blum, N., Dahn, R.D., Begemann, G., and Poss, K.D. (2011). Retinoic acid production by endocardium and epicardium is an injury response essential for zebrafish heart regeneration. Dev. Cell 20, 397-404. https://doi.org/10.1016/j.devcel.2011.

Resource



- 70. Hirose, K., Payumo, A.Y., Cutie, S., Hoang, A., Zhang, H., Guyot, R., Lunn, D., Bigley, R.B., Yu, H., Wang, J., et al. (2019). Evidence for hormonal control of heart regenerative capacity during endothermy acquisition. Science 364, 184-188. https://doi.org/10.1126/science.aar2038.
- 71. Bassat, E., Perez, D.E., and Tzahor, E. (2021). Myocardial infarction techniques in adult mice. Methods Mol. Biol. 2158, 3-21. https://doi.org/10. 1007/978-1-0716-0668-1_1.
- 72. Davarinejad, H. (2017). Quantifications of Western blots with ImageJ. http://www.yorku.ca/yisheng/Internal/Protocols/ImageJ.pdf.
- 73. Vekstein, A.M., Wendell, D.C., DeLuca, S., Yan, R., Chen, Y., Bishawi, M., Devlin, G.W., Asokan, A., Poss, K.D., Bowles, D.E., et al. (2022). Targeted delivery for cardiac regeneration: comparison of intra-coronary infusion and intra-myocardial injection in porcine hearts. Front. Cardiovasc. Med. 9, 833335. https://doi.org/10.3389/fcvm.2022.833335.





STAR***METHODS**

KEY RESOURCES TABLE

REAGENT or RESOURCE	SOURCE	IDENTIFIER
Antibodies		
Anti-EGFP, rabbit polyclonal	Thermo Fisher Scientific	Cat#: A-11122, RRID: AB_221569
Anti-EGFP, chicken polyclonal	Aves Labs	Cat#: GFP-1020, RRID: AB_10000240
Anti-DsRed, rabbit polyclonal	Takara Bio	Cat#: 632496, RRID: AB_10013483
Anti-Ki67, rat monoclonal	Thermo Fisher Scientific	Cat#: 41-5698-80, RRID: AB_11219874
Anti-Ki67, rat monoclonal	Thermo Fisher Scientific	Cat#: 14-5698-82, RRID: AB_10854564
Anti-Ki67, rabbit polyclonal	Abcam	Cat#: ab15580, RRID: AB_443209
Anti-HA tag, rabbit polyclonal	Abcam	Cat#: ab9110, RRID: AB_307019
Anti-HA tag, rabbit monoclonal	Cell Signaling Technology	Cat#: 3724S, RRID: AB_1549585
Anti-αSMA, rabbit polyclonal	ABclonal	Cat#: A7248, RRID: AB_2721021
Anti-troponin T, mouse monoclonal	Developmental Studies Hybridoma Bank	Cat#: CT3, RRID: AB_528495
Anti-troponin T, mouse monoclonal	Thermo Fisher Scientific	Cat#: MS-295-PABX, RRID: AB_61810
Anti-Cas9, rabbit polyclonal	EnCor Biotechnology	Cat#: RPCA-CAS9-Sp, RRID: AB_2744685
Anti-CD31, rabbit polyclonal	Abcam	Cat#: ab124432, RRID: AB_2802125
Anti-CD68, rat monoclonal	Biorad	Cat#: FA-11, RRID: AB_2074858
Anti-Vimentin, Chicken polyclonal	Abcam	Cat#: ab24525, RRID: AB_778824
Anti-Gapdh, mouse monoclonal	Proteintech	Cat#: sc-374117, RRID: AB_10947251
Anti-SAV1, mouse monoclonal	Santa Cruz Biotechnology	Cat#: sc-101205, RRID: AB_2184479
Experimental Models: Organisms/Strains		
Nouse: Tg(LEN-Hsp68::LacZ)	Kang et al. ¹⁰	LEN-Hsp68::LacZ
Mouse: <i>Tg(REN-Hsp68::LacZ)</i>	This paper	REN-Hsp68::LacZ
Mouse: <i>Tg(il11aEN-Hsp68::LacZ)</i>	This paper	il11aEN-Hsp68::LacZ
Mouse: Tg(Rosa26:LSL-dCas9 ^{p300})	Gemberling et al. ³⁶	Jax Strain #:033065
Mouse: <i>Tg(Rosa26:LSL-dCas9^{KRAB})</i>	Gemberling et al. ³⁶	Jax Strain #:033066
Zebrafish: <i>Tg(2ankrd1aEN-cfos:EGFP)</i>	Goldman et al. ¹⁹	pd202
Plasmids		
AAV: Hsp68::EGFP	This paper	N/A
AAV: LEN-Hsp68::EGFP	This paper	N/A
AAV: REN-Hsp68::EGFP	This paper	N/A
AAV: 2ankrd1aEN-Hsp68::EGFP	This paper	N/A
AAV: 22sema3aaEN-Hsp68::EGFP	This paper	N/A
AAV: il11aEN-Hsp68::EGFP	This paper	N/A
AAV: IN13zgc:136858-Hsp68::EGFP	This paper	N/A
AAV: LEN-Hsp68::HA-YAP5SA	This paper	N/A
AAV: cfos::EGFP	This paper	N/A
AAV: LEN-cfos::EGFP	This paper	N/A
AAV: REN-cfos::EGFP	This paper	N/A
AAV: 2ankrd1aEN-cfos::EGFP	This paper	N/A
AAV: LEN (456-662)-Hsp68::EGFP	This paper	N/A
AAV: LEN (1034-1350)-Hsp68::EGFP	This paper	N/A
AAV: 2ankrd1EN (196-644)-Hsp68::EGFP	This paper	N/A
AAV: 2ankrd1EN (405-850)-Hsp68::EGFP	This paper	N/A
AAV: CBh::EGFP	This paper	N/A
AAV: CMV::Cre	Gemberling et al. ³⁶	N/A

(Continued on next page)





Continued		
REAGENT or RESOURCE	SOURCE	IDENTIFIER
AAV: LEN-Hsp68::Cre; U6::Sav1 gRNA	This paper	N/A
AAV: 2ankd1aEN-Hsp68::Cre; U6::Agrn gRNA	This paper	N/A
Critical Commercial Assays		
Wheat Germ Agglutinin	Thermo Fisher Scientific	Cat#: W21404
β-Galactosidase Reporter Gene Staining Kit	Sigma-Aldrich	GALS-1KT
Software		
Zen	Zeiss	https://www.zeiss.com/microscopy/en/ products/software/zeiss-zen-lite.html
ImageJ	Schindelin et al. ⁵⁸	https://imagej.nih.gov/ij/
Prism 9	GraphPad	https://www.graphpad.com/scientific-software/prism/
Vevo 3100	Visual Sonics	https://www.visualsonics.com/product/imaging-systems/vevo-3100

RESOURCE AVAILABILITY

Lead contact

Further information and requests for resources and reagents should be directed to and will be fulfilled by the lead contact, Ken Poss (ken.poss@duke.edu).

Materials availability

Reagents generated in this study will be shared upon request, in certain cases following submission of a Material Transfer Agreement.

Data and code availability

All data reported in this paper will be shared by the lead contact upon request.

This paper does not report original code.

Any additional information required to reanalyze the data reported in this paper is available from the lead contact upon request.

EXPERIMENTAL MODEL AND SUBJECT DETAILS

Zebrafish

Wild-type or transgenic zebrafish of the EK/AB strain were used for all experiments. β-actin2:loxp-mCherry-STOP-loxp-DTA^{pd36},59 cmlc2:CreER^{pd1022} and 2ankrd1aEN-cfos:EGFP¹⁹ transgenic fish have been previously described. To induce ablation of CMs, adult cmlc2:CreER; β-actin2:loxp-mCherry-STOP-loxp-DTA animals were treated for 24 hours with 0.5 - 1.0 μM tamoxifen titrated to ablate ~50% of CMs.⁵⁹ Procedures involving zebrafish were approved by the Institutional Animal Care and Use Committee at Duke University.

Mice

All transgenic mice were maintained in the Duke University DLAR mouse facility. All mouse experiments were performed in accordance with federal and institutional guidelines and were reviewed and approved by the Duke, Cincinnati Children's Hospital, UCSF, and Weizmann Institute of Science IACUC committees.

Wild-type male and female C57BL/6 mice used for experiments were purchased from The Jackson Laboratory, with adults ranging in age from 8 to 12 weeks. Wild type CD-1 mice purchased from Charles River Laboratories were used to generate transgenic mice at UCSF. Male and female animals were used for experiments, with the exception of assays for CM proliferation, in which only adult male mice were used for ligation of LCA injury model.

Rosa26:LSL-dCas9^{p300} (dCas9^{p300}) and Rosa26:LSL-dCas9^{KRAB} (dCas9^{KRAB}) knock-in mice were previously described (Jax Strain #:033065 and #:033066).36 Briefly, these mice carry a CAG promoter, a loxP-flanked triple polyadenylation signal (pA) stop cassette (lox-stop-lox; LSL) and a codon optimized dCas9-p300 or dCas9-KRAB cassette with either a 1X-FLAG or 3X-FLAG, respectively. Mice were genotyped using the following primers: Forward Primer: GCAGCCTCTGTTCCACATACAC, Reverse Primer: TAAGCCTGCCCAGAAGACTC, Second F primer: AAAGTCGCTCTGAGTTGTTAT. Expected product sizes were as follows: WT band 235 bp; Knock-In 162 bp. To ensure working with the correct transgenic line, an additional PCR specific for dCas9KRAB mice was performed with primers recognizing the KRAB cassette: KRAB-specific Forward: GGCGCGCCTGCAGCCTTCAAG, KRAB-specific Reverse: GAATCAGGATGGGTCTCTTGG. Product size was 446 bp. Genotyping was performed using KAPA polymerase and the





following PCR conditions: 95°C for 1 min, 35 cycles of: 95°C for 15 seconds, 57°C for 15 seconds, 72°C for 10 minutes, and 4°C Hold. All mice used in the experiments were homozygous for $dCas9^{p300}$ or $dCas9^{KRAB}$.

METHOD DETAILS

Generation of TREE-Hsp68::LacZ transgenic mice

TREE-Hsp68::LacZ transgenic mice were generated by oocyte microinjection as described previously. 60 We subcloned zebrafish LEN, REN, and il11aEN sequences 10,19 into the Hsp68::LacZ reporter plasmid, and injected LEN-Hsp68::LacZ, REN-Hsp68::LacZ, and il11aEN-Hsp68::LacZ constructs into fertilized CD-1 strain oocytes to generate stable transgenic mouse lines. These lines were then backcrossed to C57BL/6 to expand the colony. Mice were genotyped using LacZ forward primer: TTTAACGCCGTGCGCTGTTCG, and reverse primer: ATCCAGCGATACAGCGCGTCG. Expected product size was 275 bp.

Ligation of the left coronary artery

MI injuries were performed with the assistance of the Duke Cardiovascular Physiology Core. 61 Mice (8-12 weeks) were anesthetized with ketamine/xylazine, intubated and placed on a rodent ventilator. Then, the chest cavity was entered in the third intercostal space at the left lateral border. The left atrium was gently deflected out of the field to expose the left anterior descending artery. Coronary ligation was performed by tying a suture ligature around the LCA. Following coronary ligation, the chest was closed, the pneumothorax evacuated, and the mice were extubated and allowed to recover from anesthesia.

Ischemia/reperfusion injury

To induce cardiac injury, we used a modified surgical model of ischemia with reperfusion (I/R) via temporary LCA ligation as previously described, 62 whereby 60 min of ischemia was used before inducing reperfusion, which gave more complete killing of the ischemic zone and greater reproducibility. After each surgical procedure (I/R), animals were given post-operative analgesics (buprenorphrine-sustained release formula by s.c. injection at 0.1 mg/kg) and allowed to recover until the experimental timepoints indicated, at which point mice were then further analyzed or tissues were harvested.

Skeletal muscle injury

The procedure for skeletal muscle injury in adult mice was performed as described previously.⁶³ Briefly, mice (8-12 weeks) were anesthetized with isoflurane. The skin surface of tibialis anterior (TA) muscle was shaved, scrubbed, and injected with 1.2% BaCl₂ to induce acute muscle injury.

Tibial fracture

Tibial fracture surgery was performed as described previously.⁶⁴ Briefly, mice (4 months) were anesthetized with isoflurane. An incision was made proximal to the knee to expose tibial plateau. A fracture was induced at the mid-shaft with aid of an insect pin inserted into the medullary cavity. The incision site was then closed, and mice were monitored until recovery.

Digit amputation

Adult mice were anesthetized using isoflurane. A sterile scissor was used to amputate phalanx P2 or P3 of 2nd and 4th digits. After amputation, gentle pressure was applied on the wound with gauze to stop bleeding.

AAV plasmid construction and virus production

Zebrafish regulatory sequences were subcloned upstream of an AAV construct containing a murine Hsp68 promoter and either an EGFP reporter, a mCherry reporter, or human HA-tagged YAP5SA and flanked by inverted terminal repeats (ITRs). Human YAP5SA was provided from B. Varelas (Boston University). We also used an AAV9 construct with a chicken beta actin hybrid promoter (CBh) upstream of a EGFP gene cassette, to test transduction efficiency. 65

gRNAs were designed using http://crispr-era.stanford.edu/index.jsp. 66 Four to 6 gRNAs were tested per gene. Sequences yielding highest efficiency and used for all experiments were the following: Agrn gRNA: GACTGCGCCCGCCGAGC; Sav1 gRNA: AGTTTACCGGACGTAGGCGG. An AAV backbone containing a gRNA cloning site under the control of a U6 promoter and a CMV::Cre cassette was used to clone gRNAs using the Gibson assembly method. Prior to AAV production, ITRs were verified by Smal digest. After selecting the most efficient gRNAs, the CMV promoter was excised and replaced with either a LEN-Hsp68 or a 2ankd1aEN-Hsp68 fragment using Gibson assembly. ITRs were verified by Smal digest and the resulting plasmids were used to package AAVs.

AAV vectors were produced and purified as described previously. 67 Briefly, recombinant constructs containing a pAd-DELTA F6 helper plasmid, a serotype-specific plasmid AAV2/9, and an AAV ITR plasmid containing the cassette of choice were transfected into HEK293T cells. At 72 hours after transfection, cells were harvested, purified with iodixanol gradient, and concentrated with 100 kDa filter. pAd-DELTA F6, serotype plasmids AAV2/9 and AAV plasmid vectors were provided from S. Soderling (Duke University). Small-scale AAVs were generated in Duke University laboratories, at the University of Pennsylvania Vector Core, or at the Duke University Viral Vector Core. A dose of 1 x 1011 virus particles were introduced into adult mice via tail vein injection. AAV vectors for large



Resource



scale-studies (pigs) were generated using a suspension 293 cell platform as described previously. ⁶⁸ Vector genome titers were determined using quantitative PCR with primers directed against the inverted terminal repeats (ITRs).

Histology and imaging in zebrafish

Staining for immunofluorescence was performed as described previously. Antibodies used in this study were anti-Myosin heavy chain (mouse, F59, Developmental Studies Hybridoma Bank), anti-EGFP (rabbit; Abcam), Alexa Fluor 488 (rabbit; Life Technologies), Alexa Fluor 594 (mouse and rabbit; Life Technologies). Confocal imaging was performed using a Zeiss LSM 700 confocal microscope.

Cardiac function assessed by echocardiography

For cardiac function experiments performed in Cincinnati, mice were anesthetized by 1.5% isoflurane inhalation and analyzed by B-mode and M-mode echocardiography using a Vevo3100LT instrument with a 25–55 MHz transducer (MX550D, VisualSonics). Short axis M-mode traces across the mid-papillary region of the LV were collected and LV dimensions averaged over a minimum of five consecutive cardiac cycles per heart using the LV Trace tool were analyzed to determine ejection fraction (EF) according to the formula: EF(%) = 100*[(LVED-LVES)/LVED], where LVED = [7.0/(2.4+LVIDd)]*(LVIDd)³ and LVES = [7.0/(2.4+LVIDs)]*(LVIDs)³. For cardiac function experiments performed in Durham, mice were anesthetized by 2% isoflurane inhalation and imaged by B-mode and M-mode echocardiography using a Vevo3100LT instrument with a 25–55 MHz transducer (MX550D, VisualSonics). At least 5x short axis M-mode traces of 8-10 seconds were collected across the mid-papillary region of the LV. Systole and diastole LV dimensions were measured using VevoLab's Auto LV analysis tool over 3x selected regions per M-mode recording. All measurements were averaged for each heart at each time point. Ejection fraction (EF) was calculated according to the formula above. Abbreviations, LVED, left ventricular end-diastolic volume; LVES, left ventricular end-systolic volume; LVIDd, left ventricular internal dimension at end-diastole; LVIDs, left ventricular internal dimension at end-systole.

Histology and imaging in mice

For CM cycling or dedifferentiation assays, hearts were extracted, immediately placed into ice-cold 30% sucrose, flash frozen using TFM (VWR), and sectioned at 5 μ m. Immunofluorescence staining was performed as described previously. Briefly, cryosections were fixed in 3.7% formaldehyde, permeabilized with PBS containing 0.2% Triton X-100, and blocked with PBST containing 5% normal donkey serum for 1 hour. Primary antibody was incubated overnight at 4°C. Sections were then washed and incubated with specific secondary antibodies and DAPI.

For other experiments, mice were perfused, tissues were fixed with 4% PFA, and cryo-embedded (fixation buffer containing 2% formaldehyde and 0.2% glutaraldehyde was used for X-gal staining). Fixed heart and liver samples were sectioned at 10 μm, and at 12 μm for samples stained to detect Cas9. Slides were washed in PBS, permeabilized with PBS containing 0.2% Triton X-100 for 20 minutes and blocked with 5% goat serum + 0.1% Tween in PBS (3% BSA + 0.1% Tween in PBS was used as blocking buffer for the Cas9 stained samples) for 1 hour. Primary antibody was incubated overnight at 4°C in blocking reagent. Sections were then washed and incubated with specific secondary antibodies and DAPI. Confocal images were acquired with Zeiss LSM 700 or Zeiss LSM 880 microscope. Low magnification images of mouse ventricular sections were obtained by automated tile-scan imaging. using a Zeiss 700 confocal microscope and a 10x or 20x objective. Tile-scanned z stacks were stitched using ZEN software. Antibodies used were anti-EGFP (rabbit, A11122, Life Technologies), anti-EGFP (chicken, GFP-1020, Aves Labs), anti-Ds-Red (rabbit, 632496, Clontech), anti-Ki67 (rat, 41569880, ThermoFisher Scientific), anti-Ki67 (rat, 14569882, ThermoFisher Scientific), anti-Ki67 (ab15580), WGA (W21404, Invitrogen), anti-HA (rabbit, ab9110, Abcam), anti-HA (rabbit, 3724S, Cell Signaling Technology), anti-αSMA (rabbit, A7248, ABclonal), anti-troponin T (mouse, Developmental Studies Hybridoma Bank), anti-troponin T (mouse, MS-295-PABX, ThermoFisher Scientific), anti-Cas9 (rabbit, RPCA-CAS9-Sp, EnCor Biotechnology), anti-CD31 antibody (ab124432), anti-CD68 antibody (FA-11, BioRad), anti-Vimentin antibody (ab24525), Alexa Fluor 488 (chicken, mouse, rabbit, and rat; Life Technologies), Alexa Fluor 546 (mouse and rabbit; Life Technologies), Alexa Fluor 633 (mouse, rabbit, and rat; Life Technologies). X-gal staining was performed using β-galactosidase reporter gene staining kit (Sigma). In situ hybridization was performed on 4% PFA-fixed cryosections with assistance of an InSituPro robot (Intavis).

For CM cycling and dedifferentiation assays, three sections showing the largest infarcted area were selected from each heart. Quantification analyses at the border zone (< $400~\mu m$ around infarcted area)⁷¹ were performed with 15 fields per heart imaged for Ki67 or EdU staining, and 9 fields per heart imaged for α SMA staining. Quantification analyses at distal areas were performed with 9 fields per heart imaged for Ki67, EdU or α SMA staining. The percentages of Ki67+DAPI+WGA+/DAPI+WGA+/DAPI+WGA+, or α SMA+Tnnt+/Tnnt+ cells from the three selected sections were averaged to determine a proliferation or dedifferentiation index for each heart.

Marker co-localization in mouse (EGFP, Tnnt, CD31, CD68, Vimentin) and pig tissue (EGFP, mCherry, Tnnt) was performed with Fiji. Briefly, single plane images were processed to create a binary version of one of the two channels to measure, which was subtracted and thresholded to the other to obtain a representation of co-localizing pixels only. The area of co-localizing pixels was then measured using the function Analyze > Measure, limiting the measurement to the thresholded area. Three section images of the border and 3 of the distal zone per heart were used for mouse quantifications, and 2 for pig quantifications.

For gross assessment of initial infarcts at 3 days post-injury (I/R), adult C57BL/6J mice were perfused with heparinized saline (5 units/mouse, i.p.) followed by 2% Evan's blue dye injected directly to the left ventricular chamber. Hearts were then perfused





with cold PBS before extracting and washing several times in cold PBS to remove remaining blood and dye. Hearts were then wrapped in plastic wrap and stored at -20°C for 10-15 minutes. Once frozen, hearts were horizontally cut into 2 mm intervals with a heart matrix cutting block. Heart sections were then placed in pre-warmed (37°C) 1% tetrazolium solution and incubated at 37°C for 15-20 minutes with gentle shaking. Heart sections were then transferred to freshly made 4% paraformaldehyde solution and fixed at room temperature for 15-20 minutes with gentle shaking. After fixation, heart sections were blotted dry with gauze and clamped between two glass slides for imaging. Slides were imaged with a Zeiss dissecting microscope. Images were analyzed using ImageJ with white necrotic areas demarcated by color thresholding and eye. Infarct area was calculated by the sum of white necrotic tissue area of all heart slices divided by the total tissue area of all heart slices.

For scar analysis, hearts were cut in half transversely, then were embedded with cut portions down and frozen at -80°C. Frozen sections at a thickness of 10 µm were collected from both regions using a Leica CM1950 cryostat onto glass slides. Ten sections were collected at several points along the axis of the heart, spacing collections by 500 μm. Sections were stained using Masson's trichrome and imaged using either a Zeiss Axio Zoom microscope or Zeiss Axio Imager microscope (Duke Light Microscopy Core Facility). To measure a fibrosis index, collagen/scar tissue in the left ventricular wall was traced using ImageJ software as a numerator. The denominator was calculated in most cases by tracing around the outer left ventricular wall and connecting a straight line just outside of the lumen, then subtracting the area of the lumen. Three sections representing the largest injury area were measured and averaged to give one fibrosis index value for each heart.

RNA isolation and qRT-PCR

Hearts were homogenized in Trizol using a Tissue Lyser II (QIAGEN). RNA was extracted using the standard Trizol protocol and genomic DNA removed using RNA clean and Concentrator Kit (Zymo Research/Cat#R1013), cDNA synthesis was performed using Transcriptor First Strand cDNA Synthesis Kit (Roche/Cat#04897030001) and qPCR run was performed with LightCycler 480 SYBR Green I Master (Roche/Cat#04707516001). All gene expression values were normalized to Gapdh in the same well to control for sample handling. Primers for qPCR were the following: Agm Forward: TTCGATGGTCCTTGTGACCC, Agm Reverse: AGATAGGTGTGTG TTGGGCG; Sav1 Forward: GGGAGGCACACTTCAGGTAT, Sav1 Reverse: CAGCATTCCCTGGTACGTGT; β -Actin Forward: AAGGC CAACCGTGAAAAGAT; β-Actin Reverse: GTGGTACGACCAGAGGGATAC.

Protein isolation and western blotting

For protein extraction, hearts were homogenized in RIPA buffer containing Proteinase and Phosphatase inhibitor (Thermo Fisher/ Cat#78442). Samples were denatured at 95°C for 5 min and tissue lysates were run on Mini-Protein tetra cell (Bio-Rad) using sodium dodecyl sulfate polyacrylamide gel electrophoresis (SDS-PAGE) in Tris/glycine/SDS buffer. Proteins were transferred to a PVDF membrane using Mini-Protein tetra cell in Tris/glycine buffer (v/v). Membranes were blocked for non-specific binding for 1 hour at room temperature with 3% BSA in Tris-buffered saline and Tween-20 (TBS-T) or 3% Milk in TBS-T, according to the antibody used. Membranes were then incubated with primary antibodies in the following manner: Anti-Cas9 (mouse, EnCor Biotechnology/ Cat#MCA-3F9) 1:1000 over-night (ON) at 4°C in 3% milk TBS-T; Anti-Gapdh (mouse, Proteintech/Cat#60004-1-IG) 1:500 in 3% milk TBS-T or 3% BSA TBS-T ON at 4°C;Anti-Agrn (mouse, Santa Cruz Biotechnology/Cat#sc-374117) 1:100 in 3% BSA TBS-T ON at 4°C.: Anti-Salvador (mouse, Santa Criz Biotechnology/Cat#sc-101205) 1:100 in 3% milk TBS-T ON at 4°C. After washing, membranes were incubated with Anti-Mouse HRP secondary antibody (Thermo Fisher Scientific/Cat# 31430) in TBS-T containing 3% BSA or milk at 1:50000, for 1hr RT. Proteins were visualized using Thermo Scientific SuperSignal West Dura Chemiluminescent Substrate (Fisher Scientific/Cat#34075). ImageJ were used for western blot quantifications.⁷²

Large animal studies

AAV vectors were tested in Yorkshire swine (30-40 kg) using a closed-chest, ischemia-reperfusion model of myocardial injury. Animals were pre-screened for pre-existing neutralizing antibodies.⁷³ Study protocols were reviewed and approved by the Duke University IACUC. All procedures in swine were performed under deep anesthesia using ketamine 4 mg/kg intramuscular and midazolam 0.5 mg/kg intramuscular for induction, and maintained using isoflurane 0.5-3.0% inhalation via endotracheal intubation.

Carotid artery cutdown was used for arterial access, heparin 200-300 units administered intravenously, and a 6-French sheath was inserted. Animals were administered lidocaine 3 mg/kg bolus followed by a continuous infusion 2 mg/min. Using angioplasty techniques, balloon occlusion with a 2.50-2.75 mm x 12 mm device (Emerge Monorail PTCA Dilation Catheter, Boston Scientific, Marlborough, MA, USA) of the mid-LAD for 90 minutes was performed, followed by full reperfusion to induce an anterior wall MI of the apex. ST segment elevation and frequent PVCs were observed on electrocardiogram monitoring to confirm transmural myocardial ischemia, in addition to elevation in serum troponin.

Delivery of 1 x 1014 viral particles of TREE vector to the heart was via 10-15 direct intramyocardial injections (IM) or intracoronary infusion (IC).⁷³ For IC delivery, a Judkins Right diagnostic catheter was guided from a carotid artery sheath to the left main coronary artery under fluoroscopy and the TREE vector slowly infused over 60-90 seconds. The catheter was flushed with 5 cc of normal saline to ensure infusion of all vectors from the delivery system. Completion coronary angiography confirmed patency of the left anterior descending and circumflex artery. Animals were allowed to recover from anesthesia and survive for few days to few weeks. For direct IM delivery, a right mini-anterior thoracotomy was performed to expose the apex of the heart. A 5/8" needle was used to inject 0.5 ml aliquots of viral vector into the infarct border zone and a separate remote area of the RV.







Hearts were harvested via sternotomy after systemic administration of a high potassium chloride solution to arrest the heart in diastole. Fresh biopsies were obtained from the infarct, border zone, and remote regions of the heart, and were preserved in 4% PFA along with other tissue samples for histology.

QUANTIFICATION AND STATISTICAL ANALYSIS

No animal or sample was excluded from the analysis unless viral transduction, MI, or IF staining was not performed successfully. For echocardiography measurements, only mice with ejection fraction changes from the baseline of 10% or more were included in the analyses. Quantification of CM cycling and dedifferentiation, echocardiography measurements, and scar analysis were assessed by a person blinded to the treatments. Cycling assays were performed independently by collaborators with their own reagents and animals (Figure S5F). Other experiments were not blinded during experiments and outcome assessment. Sample sizes, statistical tests, and p values are indicated in the figures or the legends. All statistical values are displayed as Mean ± Standard Deviation or Mean ± Standard Error of the Mean, as indicated in the figure legends. Statistical tests were calculated using Prism or JMP software.